12-2008

The Influence of Debris Cages on Critical Submergence of Vertical Intakes in Reservoirs

Skyler D. Allen
Utah State University

THE INFLUENCE OF DEBRIS CAGES ON CRITICAL SUBMERGENCE OF VERTICAL INTAKES IN RESERVOIRS

by

Skyler D. Allen

A thesis submitted in partial fulfillment
of the requirements for the degree

of

MASTER OF SCIENCE

in

Civil and Environmental Engineering

Approved:

_____	_____
Steven L. Barfuss Major Professor	Michael C. Johnson Committee Member
_____	_____
Joseph A. Caliendo Committee Member	Byron R. Burnham Dean of Graduate Studies

UTAH STATE UNIVERSITY
Logan, Utah

2008

ABSTRACT

The Influence of Debris Cages on Critical Submergence

of Vertical Intakes in Reservoirs

by

Skyler D. Allen, Master of Science

Utah State University, 2008

Major Professor: Steven L. Barfuss
Department: Civil Engineering

This study quantifies the influence of debris cages on critical submergence at vertical intakes in reservoir configurations. Four model debris cages were constructed of light panel material. A vertical intake protruding one pipe diameter above the floor of a model reservoir was tested in six configurations: open intake pipe, a debris grate placed directly over the intake pipe, and debris cages representing widths of 1.5*d and 2*d and heights of 1.5*c and 2*c, where d is diameter of the intake and c is height of intake above reservoir floor. A selection of top grating configurations and a submerged raft configuration were also tested for comparison.

Testing of the model debris cages indicates that the roof or top grate of a debris cage dominates the influence a debris cage has on the reduction of critical submergence of air-core vortices. The side grates of a debris cage have some influence on the

formation of vortices. The spacing of bars in the top grate has an influence on air-core vortex development.

The presence of a debris cage at vertical intakes in still-water reservoirs reduces the critical submergence required to avoid air-core vortices and completely eliminates the air-core vortex for cases where the water surface elevation remains above the top grate of the debris cage. The potential exists for designing debris cages to fulfill a secondary function of air-core vortex suppression.

(78 pages)

ACKNOWLEDGMENTS

I would like to thank the Utah Water Research Laboratory for their support, especially the faculty and staff for their assistance in preparing and conducting this research. I am most appreciative to Steve Barfuss for his insight and direction and for convincing me that I could complete this process. Thank you to my committee members, Dr. Michael Johnson and Dr. Joseph Caliendo, for their encouragement and support.

I would especially like to thank my wife, Lacey, for her motivation, support, and patience in this endeavor. I couldn't have done it without you.

Skyler D. Allen

CONTENTS

LIST OF TABLES

LIST OF FIGURES

LIST OF ABBREVIATIONS

ANSI	American National Standards Institute
ASCE	American Society of Civil Engineers
CSS	Critical sink surface
CSSS	Critical spherical sink surface
IPS3.2	Intake Pump Structure project 3.2
SNWA	Southern Nevada Water Authority
UWRL	Utah Water Research Laboratory

LIST OF SYMBOLS

A	area
C	constant
c	vertical distance from bottom of reservoir/canal to intake
C_d	coefficient of discharge
cfs	cubic feet per second, flow rate
D, d	diameter
D_f	diameter of disc or flange
fps	feet per second, velocity
Fr	Froude number, dimensionless measure of inertia
g	gravity
H, h	Head
K	viscous correction factor
L, l	length
N_υ	viscosity parameter, ratio of Re to Fr
N_Γ	circulation number
P, p	pressure
Q	flow rate
Qi	intake flow rate
r	radius
Re	Reynolds number, dimensionless measure of viscosity
Re_r	Radial Reynolds number
S	submergence, distance from intake to water surface
Sc	critical submergence
U_∞	uniform approach velocity
V	velocity
V_i	velocity at intake
V_s	velocity at CSS
V_θ	tangential velocity
W	Weber number, dimensionless measure of surface tension
z	elevation
γ	specific weight of water
Γ	circulation
ζ	vorticity
ρ	density
σ	surface tension
υ	kinematic viscosity
ψ	stream function

CHAPTER I

INTRODUCTION

This study was conducted as an extension of model study research performed for the Southern Nevada Water Authority (SNWA) in November and December of 2007 at the Utah Water Research Laboratory (UWRL). SNWA project IPS3.2 was commissioned to determine the safe operation conditions at low reservoir elevations for existing culinary water intakes in Lake Mead. A portion of the SNWA IPS3.2 project included the modeling of Intake #2, a 12 ft. diameter vertical intake with a steel debris cage to protect the intake from rock fall and debris. A scale model of the intake and its surrounding topography was constructed and tested. The approach conditions for Intake #2 introduced large amounts of circulation at the intake. During testing of SNWA Intake #2 it was observed that the presence of the debris cage resulted in significant reduction in the development of vortices at the intake as compared to the same intake without the debris cage as shown in Figure 1 and Figure 2. The purpose of this study is to determine the influence of a debris cage on the submergence required to eliminate air entraining vortices at vertical intakes.

The occurrence of vortices at hydraulic intakes can result in reduced hydraulic efficiency of the intake and increased head loss. Vortices also increase air induction and cause vibration, cavitation, unbalanced loadings, inefficient equipment operation, and slug flow from air release. These conditions can damage hydraulic machinery. Other problems associated with vortex development include non-uniform flow conditions,

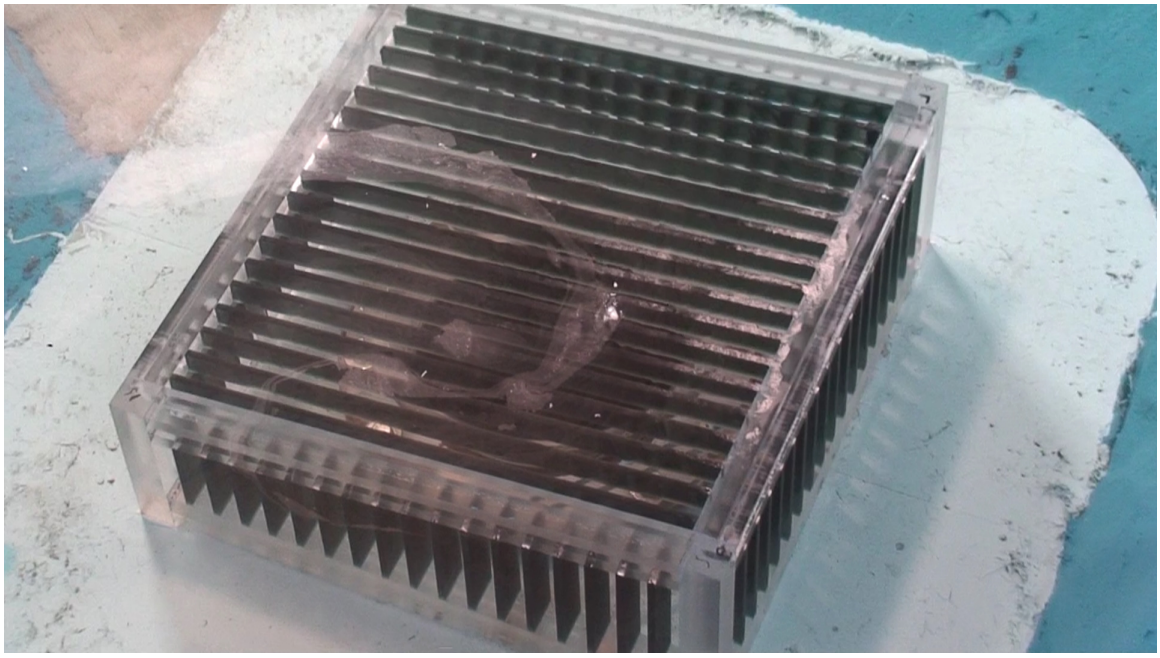

Figure 1. SNWA Intake #2 with debris cage.

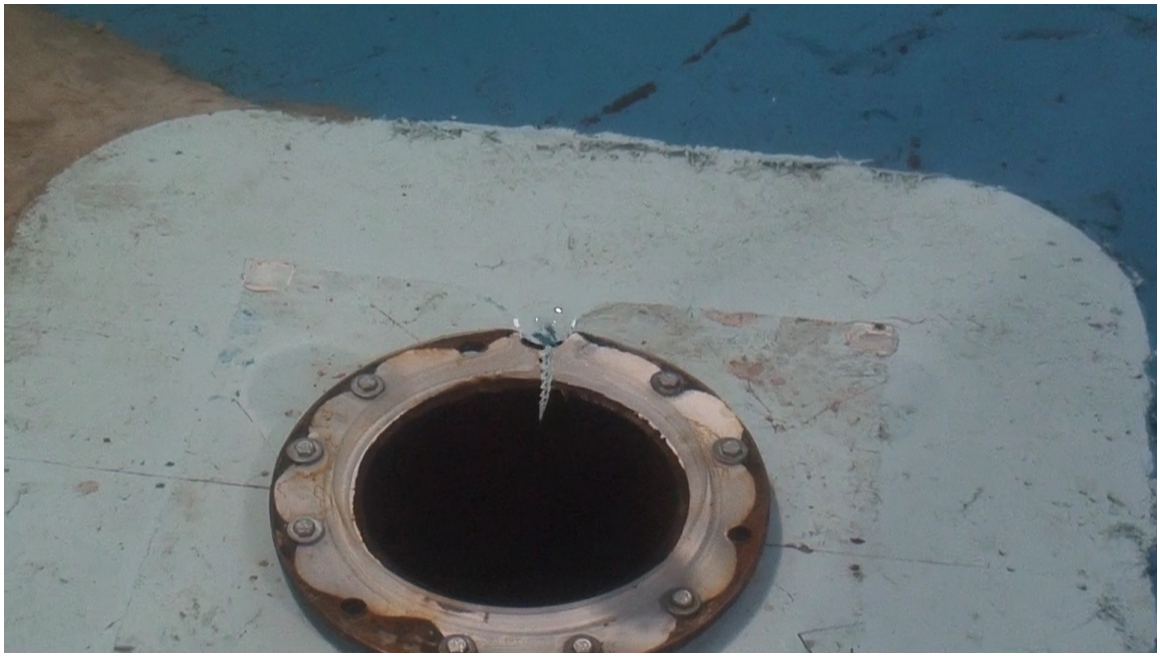

Figure 2. SNWA Intake #2 without debris cage.

drawing debris into the intake, and potential hazard for people who may venture near the affected surface region. The problems associated with vortices at hydraulic intakes can increase costs by requiring measures to correct or reduce damage to the hydraulic machinery and mitigate other risks.

The conditions which control the development of the vortex include inlet submergence, inlet flow velocities, rotation induced from approach flow paths, boundaries near the inlet, currents, and water surface conditions (waves, turbulence, etc.). As stated in the ASCE Guidelines for Design of Intakes for Hydroelectric Plants (1995) "while it is desirable to completely avoid vortex formation, the resulting design may be uneconomical." Understanding what strength of vortex is allowable will determine the expense and effort which must be expended to alter or control the conditions leading to the formation of vortices at an intake. Model studies are frequently performed to better understand the potential for vortex development at an intake and avoid over-design of intakes and are recommended by ASCE for projects where they can be justified (ASCE, 1995).

"The smallest depth at which a given type of vortex will not form" is called the critical submergence for that vortex type (Gulliver, Rindels, and Lindblom, 1986). The vortex strength which must be avoided to prevent damage, flow restrictions, or air entrainment determines the required submergence for a given intake, or the critical submergence for that intake. To prevent the formation of air entraining vortices submergence of the intake must be kept above the critical submergence for the air-core vortex. This means that small non-aerated vortices may be acceptable for the design.

Debris cages are a feature often included with hydraulic intakes to prevent large objects from being introduced into the system where they can cause damage or obstruction. Such cages are as unique as the projects they are a part of and a countless number of possibilities exist for their configuration, material, and size. In this study, model debris cages were constructed of egg crate light panel material to approximate a realistic possibility for a prototype debris cage. The debris cages constructed for use in this study were intended to represent generic debris cages and were not intended to represent any specific design.

The assumption of still water is used by several researchers for analysis of vortices in reservoir intake conditions to simplify the process (Yildirim and Jain, 1981; Gulliver, Rindels, and Lindblom, 1986). A real reservoir is not likely to be still water, since surface waves, density stratification, currents, and flow to intakes will exist in the reservoir. However, the assumption of still water will be conservative, since the influence of waves and flow variations will have the effect of disrupting vortex formation.

Vortices at hydraulic intakes are a common concern for designers. The presence of a vortex can result in reduction of efficiency of the intake, vibration, air induction, and damage to hydraulic machinery. In most hydraulic intakes it is desirable to operate without the presence of a vortex. For hydraulic engineers it is important to be able to predict the formation of vortices from an understanding of the hydraulic conditions at an intake. Model studies are frequently performed to assist designers in creating the proper conditions to avoid development of vortices. A better understanding of how debris cages

help to control vortex development is necessary to improve the capacity of designers to use them as vortex control structures.

CHAPTER II

LITERATURE REVIEW

Proper understanding of the mathematical theory of vortices and the physical properties of vortices aids in comprehension of the physical characteristics and behavior of vortices. A brief description of some of the general equations and characteristics defining vortices that are applicable to this study is presented to benefit the reader.

Vortex Development

Daugherty and Franzini (1977) state that there is no expenditure of energy in a free vortex, the fluid rotation is a result of internal action or rotation imparted by the flow. The free surface vortex is irrotational. No energy is imparted to the fluid so head is constant as expressed in the Bernoulli equation.

$$H = \frac{p}{\gamma} + z + \frac{V^2}{2g} = \text{constant} \tag{1}$$

Streamlines in a cylindrical free vortex form concentric circles with constant angular momentum along each streamline as expressed in Equation 2.

$$V \cdot r = C \tag{2}$$

The streamline for a cylindrical free vortex forms a closed circular path. The expression of the stream function is shown in Equation 3.

$$\psi = \int V \cdot dr \tag{3}$$

The cylindrical free vortex expresses the circumferential component of the vortex flow in the case of a vortex entering a drain hole. If radial flow is superimposed on the cylindrical flow described above, the flow lines become spiral in shape. This describes the case of a point sink combined with circulation.

Circulation (Γ) is the line integral of the velocity around a closed path shown in Equation 4.

$$\Gamma = \oint_L V \cdot dL \tag{4}$$

Vorticity (ξ) is the circulation per unit of enclosed area as described in Equation 5 and expresses the intensity of circulation.

$$\zeta = \frac{\Gamma}{A} \tag{5}$$

A detailed description of a free surface vortex using Euler's equations in cylindrical coordinates with continuity and steady flow assumptions can be found in Anwar (1965) but is not addressed here. Anwar (1965) explains the difficulty in measuring the velocity distribution in the body of the vortex. When small current meters were inserted into the flow it created sufficient disturbance to disrupt the vortex. The solution was found using a telescope and rotating prism to track particles from light reflection. Other methods, such as 3-D laser velocity metering, could be employed to measure the velocities within the vortex without disturbance but were not applied in this study.

Anwar (1965) found that "a strong vortex behaves as a vortex tube in an inviscid fluid, with a slight modification due to viscosity." He presents two theorem to apply to air-core vortices: 1) "A circulation has the same value for all closed curves embracing the vortex tube, i.e., a vortex tube will either form a closed ring, or must start and terminate on a fixed boundary to the flow." In the case of a free surface air-core vortex, this means that the vortex must extend from the free surface to the intake. 2) "No flow can occur across a vortex tube. This implies that there is no radial flow within the vortex tube." Energy lost to viscosity must be replaced since it is not truly an inviscid fluid. This energy comes from a small axial flow.

In a later paper Anwar (1968) stated:

> A strong or a weak vortex can only form at an intake when swirl and head above the intake reach certain values; otherwise only small depressions or a dimple will be formed on the water surface which will not extend to any depth and cause vibration in the pipeline or reduce the coefficient of discharge. Such a weak spiral flow, however, may reduce the efficiency of the hydraulic machinery. (p. 393)

Tests by Posey and Hsu (1950) which measured the influence of a vortex on the discharge coefficient of a vertical intake concluded that the presence of a strong vortex could cause a nearly 80 percent reduction in the coefficient of discharge for the orifice.

Anwar (1968) notes that the fluctuations of vortices that grow on energy obtained from others, or decay on account of breaking up or by molecular viscosity do not seriously affect the efficiency of the intake and hydraulic machinery or cause significant

vibration. The conclusion is that only stable vortices result in energy loss, reduction in discharge, and vibration in pipelines.

Tangential velocities measured at various levels and radii by Anwar showed that the tangential velocity depends on radius only for a given flow. The expression of this conclusion shown in Equation 6 is in agreement with the ideal flow of a free vortex (compare to Equation 2).

$$V_\theta \cdot r = C \tag{6}$$

Close to the air-core (<4") the tangential velocity departs from this distribution and is less than that predicted. The free surface profile of a steady air-core vortex was determined by Anwar to be hyperbolic in the air-core until the profile approaches the free surface at an angle of nine to eleven degrees. Beyond this point the profile can be calculated using a different method detailed by Anwar (1968).

Important dimensionless parameters with significance to vortex development considered by Gulliver, Rindels, and Lindblom (1986) include:

Dimensionless submergence S/d

A circulation parameter $N_\Gamma = \Gamma S/Q$ N or $N_\Gamma = \Gamma d/Q$

Froude number $Fr = V/\sqrt{gd}$ or $Fr = V/\sqrt{gS}$

Reynolds number $\mathrm{Re} = Q/\upsilon S$ or $\mathrm{Re} = Vd/\upsilon$

Weber number $We = \rho V^2 d/\sigma$ or $We = V^2 S/\sigma$

where V = intake velocity, d = intake diameter, g = acceleration of gravity, Q = intake discharge, Γ = circulation, ρ = density, υ = kinematic viscosity, and σ = surface tension. It is noted that vertical intakes have a greater tendency for development of free surface vortices than other intake orientations and that approach flow path has a significant impact on vortex development.

Critical Submergence

The ASCE publication "Guidelines for Design of Intakes for Hydroelectric Plants" (1995) states that "vortices are classified into two types; air-core and dye-core." The dye-core vortex can be visually observed by using some kind of tracer in the flow and describes coherent swirl in the fluid which extends into the intake. Injecting tracer into the flow results in the tracer being collected into the swirling vortex when the dye-core vortex is present. The air-core vortex can be observed visually when air bubbles or an open air-core at the axis of the vortex extends into the intake.

Critical submergence is defined by Gulliver, Rindels, and Lindblom (1986) as "the smallest depth at which a given type of vortex will not form." For many practical applications the limiting vortex type is the air-core vortex. For Jain, Ranga Raju, and Garde (1978) and Yildirim and Kocobas (1995, 1998) the air-core vortex was defined as the limit for critical submergence. For many cases, including testing performed by Yildirim and Kocobas (1995, 1998) and Jain, Ranga Raju, and Garde (1978) the critical submergence is defined as the depth when the air-core vortex just reaches the mouth of the inlet. Another vortex condition could define the critical submergence as determined

by the limiting flow conditions at the intake as determined by the designer. The critical condition for this study was defined as the air-core vortex. As recommended by Hecker (1981) the critical vortex may also be the dye core vortex where coherent swirl extends to the intake. Hecker (1981) suggests that for conditions where vortices must be avoided, the dye core vortex is a safe limiting condition with the dye core vortex present less than 50 percent of the time.

Model Scale Effects

Hecker (1981) notes that hydraulic scale models are frequently scaled using Froude similarity since the predominant forces are typically inertia and gravity. Surface tension and viscous forces cannot be reduced simultaneously as much and can result in "scale effects". Scale effects result when the relatively higher surface tension and viscosity in the model influence the flow characteristics, leading to model testing which does not accurately reflect prototype flow characteristics.

A paper by Hecker (1981) provides a synthesis of results from several previous researchers and analysis of results from a collection of model study results yielded some interesting conclusions regarding scale effects and the effectiveness of using Froude scaling for vortex model studies. Hecker notes that vortices are subject to prediction errors resulting from the impossibility of reducing all influencing forces by the same factor. The predominant forces are inertia and gravity which can be reduced by Froude scaling. As stated by Hecker (1981), "viscous and surface tension forces cannot simultaneously be reduced as much," resulting in scale effects. Studies referenced by

Hecker (Anwar, 1965; Dagget and Keulegan, 1974) conclude that if Reynolds number based on inlet flow and submergence or intake diameter is maintained greater than $3x10^4$ then Froude scaled flows will avoid viscous scale effects on air-core vortices (see Equation 7)

$$\mathrm{Re} = \frac{VL}{\upsilon} \geq 3x10^4 \tag{7}$$

where Re is Reynolds number, V is velocity, L is length or intake diameter, and υ is kinematic viscosity.

According to Hecker, some researchers have suggested testing models at higher than Froude scaled intake velocities, even up to prototype velocities, to avoid scale effects in air-core vortices. This technique is concluded to be useful for a limited range of model scales from about 1:3 to 1:8 since increased velocities creates approach conditions which are not similar to the prototype. Hecker (1981) notes that "for some scale ratios, the use of the equal intake velocity concept would seriously undermine the primary Froude scaling criterion used to achieve proper approach flow patterns and the resulting circulation at the intake. In some of the tests cited by Hecker the use of the equal velocity method was found to produce exaggerated results or to create increased turbulence and wave action which could disrupt vortices.

Scale effects resulting from surface tension are difficult to isolate due to the interrelationship between Weber and Reynolds numbers. Some research has shown that surface tension effects on air-core vortices may not be negligible. Hecker concludes that "the question of surface tension effects is considered unresolved." Scale effects from

surface tension and viscous forces are greater on air-core vortices than surface dimples. If scale effects from viscosity and surface tension are influencing the vortex then the transition from surface dimple and coherent swirl to air-core vortex will be more rapid in the prototype than observed in the model.

Experiments by Anwar found that similarity for narrow air-core vortices or deep surface dimples was not dependent on radial Reynolds number for

$$\mathrm{Re}_r = \frac{Q}{\nu h} \geq 10^3 \tag{8}$$

where Re_r is radial Reynolds number or Reynolds number with h equal to the radius of the intake, Q is intake flow, and υ is kinematic viscosity. Similarity for strong open core vortices is dependent on Reynolds number. The conclusion drawn is that the roughness of boundaries influences the development of strong open core vortices and that "the radial flow at the boundary supplies the energy necessary to maintain an open vortex, without which it would collapse to produce a dimple at the water surface" (Anwar, 1968). This means that by altering the roughness of boundaries influencing the circulation, vortex development can be controlled. The strength of an open vortex can be reduced by either increasing submergence or reducing circulation. Circulation can be reduced by roughening boundaries or altering approach geometry (Anwar, 1968). Geometric and dynamic similarity of a hydraulic model to the prototype can be achieved through Froude scaling for vortex models of scale not less than 1:20 (Anwar, 1968).

Investigation by Jain, Ranga Raju, and Garde (1978) comparing water and water diluted with cepol (carboxyl-methyl cellulose), to obtain a comparison of fluids with the

same kinematic viscosity but different surface tension revealed that surface tension, does not affect the development of the air entraining vortex. This was true for

$$120 \le W \le 3.4x10^{4}$$
$$W = \rho V^{2} d \Big/ \sigma \tag{9}$$

where W is Weber number as defined in the equation, ρ is the density of water, d is intake diameter, V is intake velocity, and σ is surface tension of water.

Further comparison of water and water diluted with iso-amyl alcohol to maintain the same surface tension with different kinematic viscosity found that the kinematic viscosity did have an effect within a specific range. Jain, Ranga Raju, and Garde (1978) determined the limit for the ratio of Reynolds number to Froude number (N_v) above which the viscous effects become negligible as shown in Equation 10.

$$N_v = g^{1/2} d^{3/2} \Big/ \nu \ge 5x10^{4} \tag{10}$$

where g is acceleration due to gravity, d is intake diameter, and υ is kinematic viscosity.

A correction factor for predicting viscous effects is further detailed in the study. Jain, Ranga Raju, and Garde (1978) further determined that model prototype similarity in circulation could be maintained by ensuring geometric similarity using Froude scaling.

Gulliver, Rindels, and Lindblom (1986) stated that with proper design the Reynolds and Weber numbers (viscous and surface tension effects) are not significant

factors. Froude number and circulation (N_Γ) greatly influence vortex development and the required submergence.

A summary of model-prototype observation comparisons is presented by Hecker (1981) and demonstrates that in many cases the observation of vortex intensity in models do not always translate directly to the intensity of vortex observed in prototypes. Factors which contribute to these observational differences are presented as including insufficient attention to approach geometry, topography, and boundary roughness in the model, viscous scale effects on flow devices such as screens, wind currents, and density stratification in the prototype. Comparisons of model-prototype observations revealed that for Froude scaled models with Fr = 1 model vortex strength was typically consistent with vortex strength observed in the prototype. However, some cases were found where prototype vortices were stronger or more persistent than in the model. For models scaled with velocity Froude scaling between 2 and 4.5, the model vortex observations are similar to or stronger than those observed in the prototype. For this study no alteration was made and all dimensions were scaled using Froude scaling.

Vortex Suppression Methods

Hecker (1981) suggests that models with vortex suppression devices may dissipate excessive energy due to the relatively low Reynolds number resulting in under-prediction of the vortex in the model study. Such viscous scale effects should be considered in situations where they may be a factor.

Research by Gulliver, Rindels, and Lindblom (1986) consider the design requirements of an intake to avoid free surface vortex development. They state that for pump intakes the dye core vortex, coherent swirl into the intake, is the limiting vortex condition for optimal operating conditions. Gulliver, Rindels, and Lindblom also note that for an intake with a long penstock a small amount of swirl may be eliminated by pipe friction. This indicates that some degree of vortex may be permissible at the intake.

Gulliver, Rindels, and Lindblom (1986) consider various methods of reducing vortex development at intakes. Successful among these are submerged rafts including grating near the intake used as debris racks, reduction of intake velocity by increasing intake area, headloss devices, and improvement of approach flow paths to reduce circulation. It is recommended that for installations where vortex development is a concern, a model study be conducted to more accurately assess vortex development for the intake and determine possible solutions.

Prediction of Critical Submergence

Jain, Ranga Raju, and Garde (1978) determined that the development of the air entraining vortex is related to the circulation number (N_Γ), Froude number, and viscosity parameter (N_v) as follows:

$$K\frac{S_c}{d} = 5.6N_\Gamma{}^{0.42}F^{0.50}$$
$$N_\Gamma = \Gamma S_c \big/ Q \qquad (11)$$

where K is the correction factor for viscous effects, equal to 1 for N_v>5x10^4, S_c is critical submergence, d is intake diameter, N_Γ is circulation number, F is Froude number, Q is intake flow, and Γ is circulation.

A recent study by Yildirim and Kocabas (1995) applied the potential flow solution for the combination of a point sink and uniform canal flow to describe the critical submergence of a vertical intake. By dimensional analysis and applying criteria from other researchers the dimensional variables of influence were reduced to the following:

$$\frac{S_c}{D_i} = f\left(C_d \frac{V_i}{U_\infty}, \frac{c}{D_i}, \frac{D_f}{D_i} \right) \tag{12}$$

where S_c is critical submergence, D_i is intake diameter, C_d is orifice discharge coefficient, V_i is intake velocity, U_∞ is uniform approach velocity, c is distance from reservoir bottom to intake elevation, and D_f is disc or flange diameter if present.

From their experiments with uniform approach flow and varying intake configurations, Yildirim and Kocabas (1995) concluded that the critical submergence could be predicted by using the critical sink surface (CSS) defined by the radius of the Rankine half-body of revolution. The Rankine half body of revolution divides the flow into the regions of flow entering and not entering the intake. The equation for the solution of the Rankine half-body of revolution is referenced by Yildirim and Kocobas as follows:

$$r = \sqrt{\frac{Q_i}{2\pi U_\infty} \cdot (1 - \cos\theta) \cdot \frac{1}{\sin\theta}} \tag{13}$$

where r is radial distance from point sink (center of intake), Q_i is intake flow, U_∞ is uniform approach velocity, and θ is the angle between the horizontal axis and radial direction vector. Using this equation for the vertical distance directly above the intake the sin and cos terms are eliminated from the equation. Substituting Q as defined into Equation 13 and equating critical submergence (S_c) to r, the resulting definition for the dimensionless critical submergence is shown in Equation 14.

$$\frac{S_c}{D_i} = \frac{1}{2\sqrt{2}} \cdot \left(C_d \frac{V_i}{U_\infty} \right)^{1/2} = 0.354 \cdot \left(C_d \frac{V_i}{U_\infty} \right)^{1/2} \tag{14}$$

where S_c is critical submergence, D_i is intake diameter, C_d is orifice coefficient of discharge, V_i is intake velocity, and U_∞ is uniform approach velocity. A 10 percent variation between the critical submergence predicted by this equation and that observed during testing was noted by Yildirim and Kocabas resulting from surface tension, viscosity, gravity, and circulation effects since real flows are not completely inviscid as the theory assumes. A correction factor of approximately 10 percent was applied to accommodate the variation resulting in Equation 15

$$\frac{S_c}{D_i} = 0.4 \cdot \left(C_d \frac{V_i}{U_\infty} \right)^{1/2} \tag{15}$$

where S_c is critical submergence, D_i is intake diameter, C_d is orifice coefficient of discharge, V_i is intake velocity, and U_∞ is uniform approach velocity.

These results apply to $S_c/D_i > 0.5$ and $C_d V_i/U_\infty > 2$. Yildirim and Kocobas (1995) state that extremely slow uniform canal flow can be approximated as a still-water body as described by other researchers including Yildirim and Jain (1979) and Gulliver, Rindels, and Lindblom (1986). In later research Yildirim and Kocabas (1998) confirmed that the potential flow solution was also applicable to still water reservoir conditions using Equation 16.

$$\frac{S_c}{D_i} = \frac{-\left(c/D_i\right) + \sqrt{\left(c/D_i\right)^2 + \left(V_i/2V_s\right)}}{2} \tag{16}$$

where S_c is critical submergence, D_i is intake diameter, c is height of intake above reservoir floor, V_i is intake velocity, and V_s is the critical velocity at the critical spherical sink surface (CSSS). For the case of still-water the critical sink surface is a sphere excluding the blockage area of the sphere intersecting the lower surface. In the case where $c \geq S_c$, c is taken to be equal to S_c. V_s is a function of flow rate. Therefore a plot of area of CSSS v. Q_i was created by Yildirim and Kocobas for each test configuration and V_s is the value of the slope of the resulting line to use in Equation 16.

The prediction equation presented by Jain, Ranga Raju, and Garde (1978) (Equation 11) has the difficulty of relying on known circulation values for calculating critical submergence. Circulation is difficult to measure and extremely difficult to predict during initial design of an intake. The equation presented by Yildirim and

Kocabas (1998) (Equation 16) does not include a circulation parameter as it was developed specifically for radial approach flows. The Yildirim equation most closely matches the conditions tested in this study and is compared to the test data in subsequent chapters.

CHAPTER III

MODEL AND DATA COLLECTION

Testing was performed to determine the specific critical depth of a scale model intake and compare directly to the same intake with several model debris cages and grating types. From the modeled data, a comparison of the resulting influence on the critical submergence of the intake was made.

Model Setup

Testing was conducted in an 18-ft x 18-ft x 5-ft reservoir box on an elevated platform (see Figure 3). A 12-inch diameter steel pipe with a square edged inlet was installed vertically in the test box with the inlet 12 inches above the floor of the box (see Figure 4). Eight-inch and 20-inch supply lines controlled with butterfly valves entered the box and supplied flow to diffuser piping which delivered flow to three sides of the box (see Figure 5). Inflow passed from the diffuser piping through a baffle wall covered with filter fabric to dissipate waves and create uniform approach velocities (see Figure 5).

The supply lines were monitored using U-tube manometers with either mercury or blue fluid measuring the pressure differential of orifice plates located in the eight inch and twenty inch supply lines. Manometer readings were taken to a precision of 0.05 cm. Inflow from the supply lines was computed using information from calibrations previously performed at the UWRL and the manometer readings (see Appendix C).

Figure 3. Test reservoir box.

Figure 4. 12” diameter intake pipe.

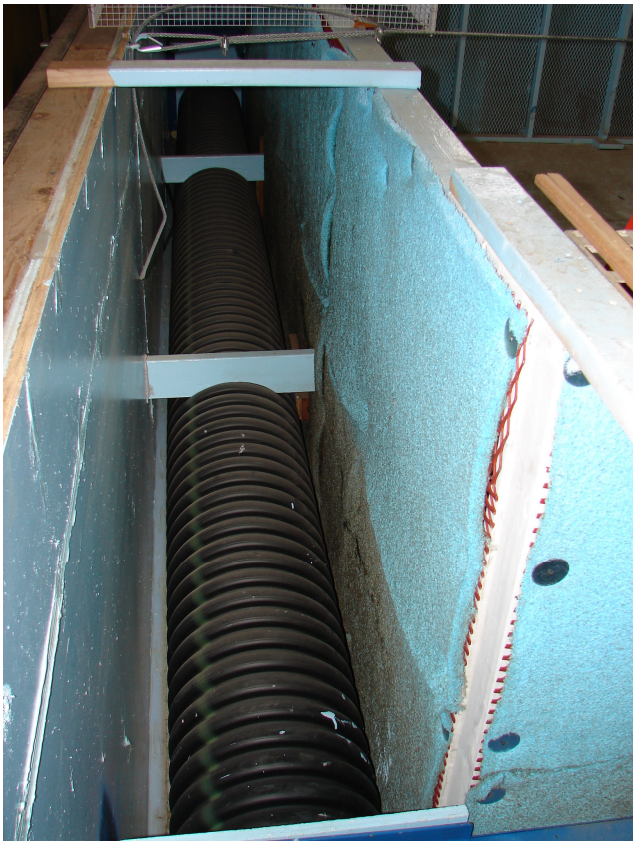

Figure 5. Diffuser and distribution piping.

Outflow was controlled using a butterfly valve mounted in the 12-inch pipe. Outflow was freely discharged to prevent backwater effects on the inlet and was not measured (see Figure 6).

Reservoir elevations were measured with a piezometer located on the side of the box with a scale affixed and read to a precision of 0.05 inches (see Figure 7). Plastic tubing was used to connect the piezometer to a small hole in the floor of the reservoir several feet away from the inlet where reservoir velocities were negligible.

An adjustable rectangular weir was cut in the side of the box to allow for increased control of the water surface elevation and reduce the time required to reach a

Figure 6. Outflow control valve.

Figure 7. Reservoir piezometer with measurement scale.

steady-state condition (see Figure 8 and Figure 9). The weir was calibrated to determine the coefficient of discharge (C_d) for Equation 17

$$Q = \frac{2}{3}\sqrt{2g}C_d L H^{3/2} \tag{17}$$

where Q is flow (cfs), g is acceleration due to gravity, C_d is the weir coefficient of discharge, L is weir length of 3 inches or 0.25 feet, and H is head above the weir crest in feet. Weir calibration data and results are detailed in Appendix A. Weir outflow was computed using the difference between observed reservoir height and weir height for the value of head (H) in Equation 17. Using continuity and the known inflow and the outflow over the weir, outflow through the pipe was computed (Appendix C).

Model debris cages were constructed of egg crate styrene light panels (see Figure 10). The debris cages were not intended to represent any specific design, but to approximate a general configuration of a debris cage over an intake. The cages were constructed in dimensions shown in Table 1. Cage dimensions were selected to achieve vertical distance from the intake to the top of the cage of 0.5*c and 1*c and horizontal distance from the center of the intake to the sides of the cage of 2*d and 3*d where c is the height of the pipe invert above the bottom of the reservoir and d is the diameter of the intake pipe. Cage configurations are referred to by the dimensions of the debris cages in inches in the following format: W-in x D-in x H-in. The additional two configurations were a plate of the same light panel material placed directly on the mouth of the inlet and the open pipe, referred to as the plate configuration and the open configuration, respectively.

Figure 8. Overflow weir outside.

Figure 9. Overflow weir inside.

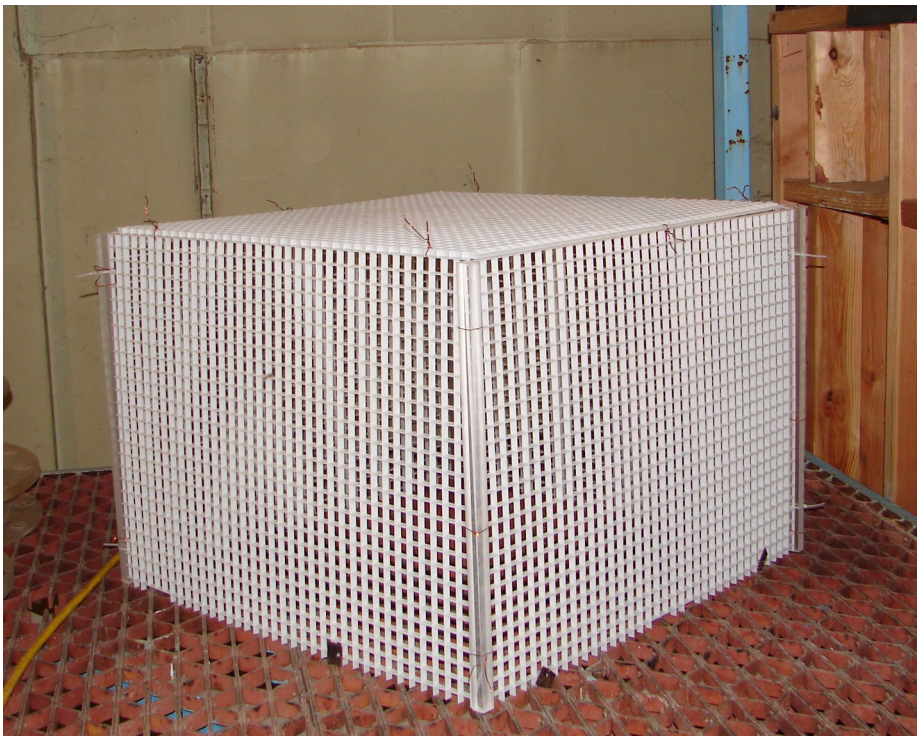

Figure 10. Styrene light panel model debris cage, 24”x24”x24” cage.

Table 1. Model debris cage dimensions

Debris Cage	width/depth factor *d	width (in)	depth (in)	height factor *c	height (in)	height above intake (in)
24x18	2	24	24	1.5	18	6
24x24	2	24	24	2	24	12
36x18	3	36	36	1.5	18	6
36x24	3	36	36	2	24	12

A few additional tests were performed using the 24-in x 24-in x 18-in debris cage and varying the configuration of the top grate. Six different top grate configurations were tested for comparison. Three top grates made of light panel material with portions broken out were used. The light panel grating forms a grid of 5/8" x 5/8" spaces. The panels bracing pieces were broken out to form 2x2 open squares, 3x3 open squares, and 6x6 open squares. Additionally, three slats of light panel material two grid spaces in width were tested in three configurations. The first configuration of light panel slats parallel with equal spacing, leaving spaces of about 5 inches between each. The second configuration was a single slat across the center. The third configuration was a cross (see Figure 11). Results are presented in Appendix C.

One additional test was conducted representing a submerged raft configuration. A 24-in x 24-in x 18-in piece of light panel grating was suspended over the intake at the same elevation as the top grate on the 24-in x 24-in x 18-in debris cage (see Figure 12). Results are presented in Appendix C.

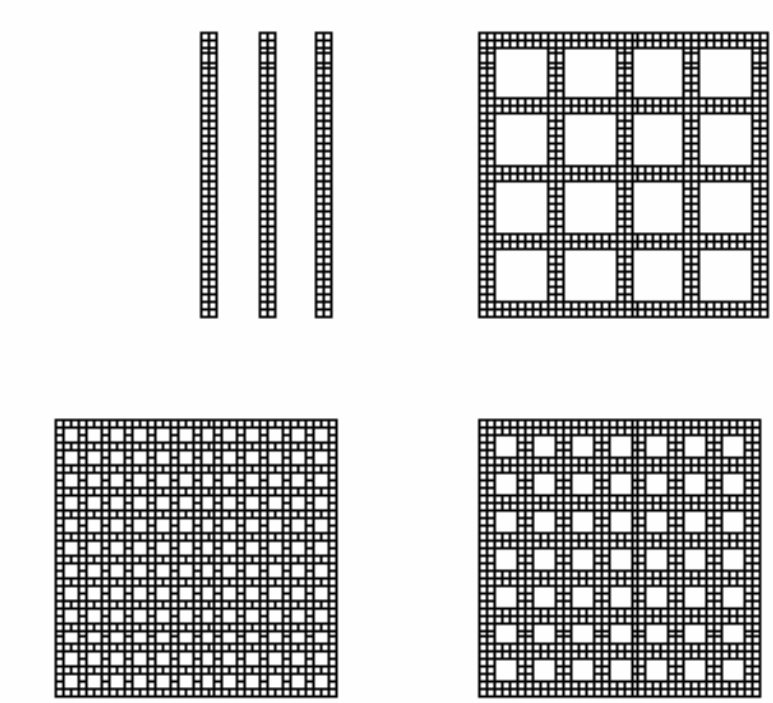

Figure 11. Top grating variations: clockwise from upper left: slats, course grating, medium grating, fine grating.

Figure 12. Submerged raft configuration.

Testing Methodology

The model was tested at each of the six different configurations for five different flow rates; 0.92, 2.08, 2.95, 3.61, and 4.25 cfs. Two to three different outflow conditions for each flow rate were established and allowed to stabilize. Outflow conditions, and consequently the model reservoir pool, were varied by changing both the outflow butterfly valve and the overflow weir height. Tests were performed to exhibit an air-core vortex in the open configuration (no debris cage) as a base condition to enable comparison of the vortex suppression effects with each cage configuration installed. Some of the tests for the open configuration resulted in reservoir elevations near the critical submergence for the air core vortex. Each test resulted in a reservoir elevation, intake flow rate, and observations of the surface effects. Flow velocities in the model reservoir approaching the intake typically were about 0.10 ft/s, although they varied depending on the reservoir depth and flow rate. Flow did not deviate from the desired uniform radial flow during any of the test scenarios.

Target inflows were selected to produce a reasonable range of scaled flows. Scale factors discussed previously restrict vortex models to larger scales. Anwar (1965) suggests a limit of 1:20 for Froude scaled models. The test model was not designed to be a specific scale. The selected flow values represent scaled prototype inlet velocities ranging from V_p=1.17 ft/s at a 1:1 scale with Q_m=0.92 cfs to V_p=24.2 ft/s at a 1:20 scale for Q_m=4.25 cfs. This range of velocities can be considered the range of applicable values for this research. The range of represented velocities is therefore 1.17 to 24.2 ft/s. It would be exceptional for an intake to exceed this range. Intake velocities typically may

range from two to twenty fps, however, velocities on the order of eight to twelve ft/s are much more common (ASCE, 1995).

To ensure that the testing results were not subject to scale effects, as discussed previously, Reynolds, Weber, and Froude numbers were computed for each test and compared to the criteria set forth by previous researchers. Reynolds numbers for results presented in this study ranged from 5.54×10^4 to 2.79×10^5, all values greater than the 3×10^4 limit recommended by Hecker (1981) (Equation 7). Weber numbers ranged from 429 to 1.09×10^4, all values within the range recommended by Jain, Ranga Raju, and Garde (1978) of 120 to 3.4×10^4 (Equation 9). The value of the parameter N_υ (Equation 10) was 2.94×10^5, greater than the limit outlined by Jain, Ranga Raju, and Garde of 5×10^4. It can be concluded that, based on criteria outlined by previous researchers for avoiding model scale effects for surface tension and viscous forces, no model scale effects should exist for the vortex flow modeling in this research.

The strength of vortices can be categorized based on observed characteristics. Previous researchers have created scales for classification of vortex strength (i.e. Knauss, 1987). For this study specific categorization of vortex strength was not attempted, rather a continuum of vortex strengths was described using both qualitative and quantitative properties of the vortex. Observed properties included visible circulation described from mild to strong, surface dimple size described from small to large and often measured as a diameter to precision of ½-inch during testing, size of vortex core described from very small to large and distinguishing between vortex cores which extended to the inlet and those that extended only slightly below the surface dimple. Comparison of these

observed properties offers an understanding of the relationship between vortex strength in the different test configurations.

It was observed during testing of SNWA Intake #2 and during preliminary testing for this study that during vortex development a condition occurs where the vortex fluctuates in strength, the tip extending toward the inlet then retracting to a point much closer to the surface. In testing for this study it was found that the angle of observation combined with refraction from the water made accurate viewing of the depth of the vortex tip relative to the inlet difficult. The critical submergence in this study was measured at the point when the vortex just begins to extend to greater depths. The critical vortex was defined as the air-core vortex which extends to a depth greater than two to three inches. This condition for the critical vortex was chosen to facilitate observation precision. During testing it was found that this condition immediately precedes the full development of the air-core to the inlet. A small decrease in water surface elevation is all that is required to stimulate the transition of the tip of the vortex air-core from a few inches below the surface to extending to the inlet. This assumption is supported by the discussion by Anwar (1965) of a strong vortex acting as a vortex tube. The vortex must either be a surface dimple, or extend to the inlet. The many observations of air-core vortices draw particles into the flow and the time often required to draw a particle down into the intake supports the theory of a vortex tube with small axial flow.

A photo of the vortex near the critical submergence point is shown in Figure 13. The vortex is unstable at the critical submergence point. Very few data points were classified as being at critical submergence, rather they were classified as air-core vortex

occurring or air-core vortex not occurring. By so doing, a range of flow conditions was tested from which the critical submergence could be determined. A complete summary of test results is found in Appendix B.

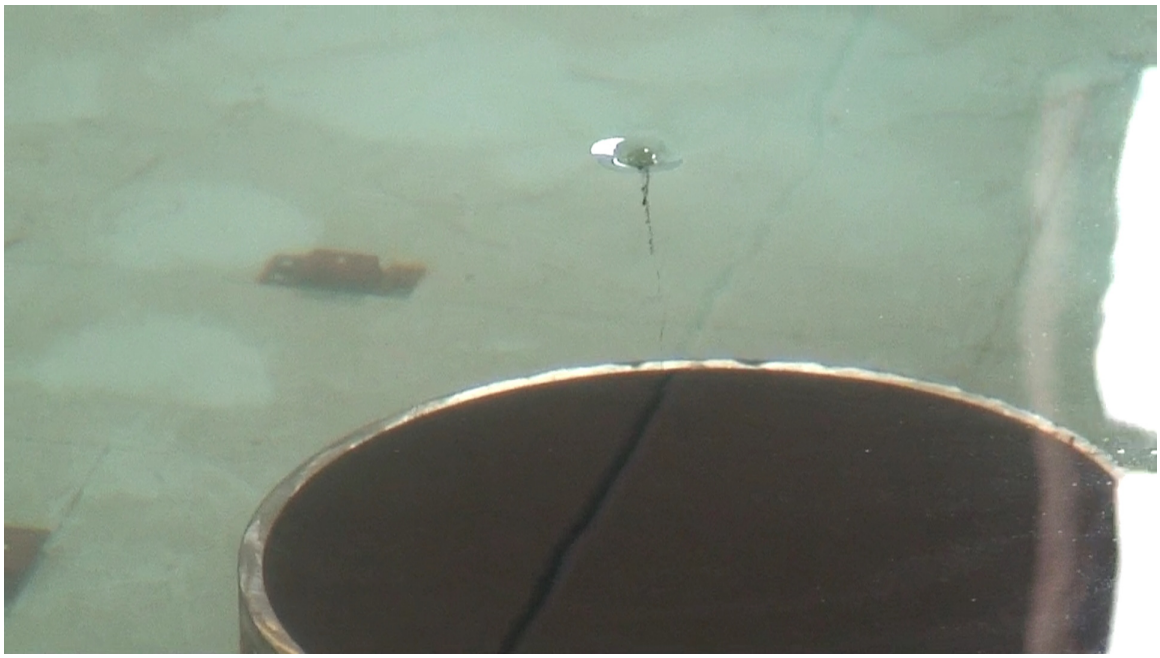

Figure 13. Vortex near critical submergence.

CHAPTER IV

TEST RESULTS AND ANALYSIS

Open Configuration Results

Testing for the intake in the open configuration (no debris cage) yielded eight data points where an air-core vortex was observed, three points which approximate the critical submergence for the air-core vortex, and one point where no air-core vortex was observed. The plot of these results is shown in Figure 14.

A curve was fitted to approximate the critical submergence conditions for the open configuration. The critical submergence boundary occurs in the region between data points where no vortex was observed and those where a vortex was observed. In the

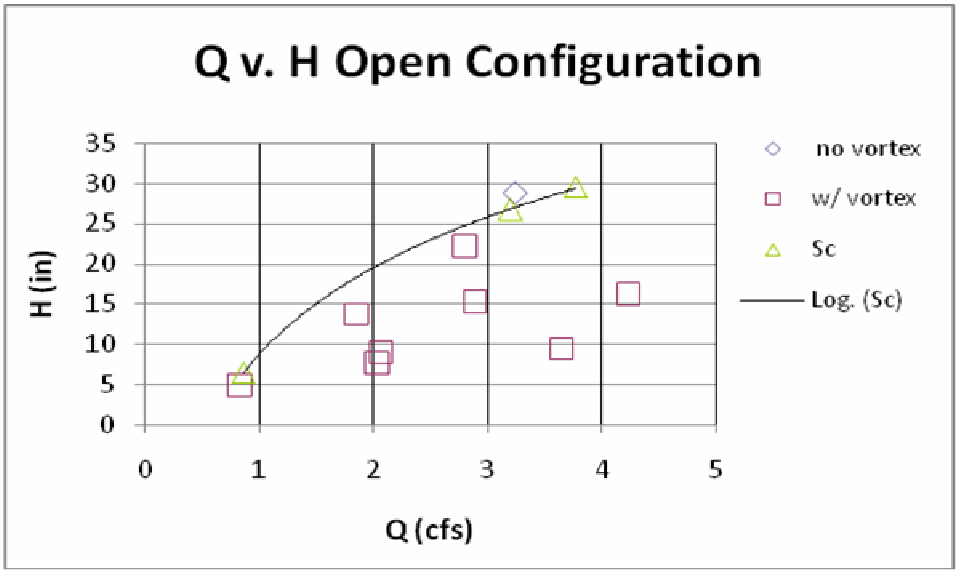

Figure 14. Open configuration results.

open configuration the placement of this boundary is aided by the observation of points near critical submergence. Figure 15 shows a typical operating condition for the open pipe configuration with air-core vortex established.

Comparison to Predictions from Theory

Testing results for the open configuration were compared to two different theoretical critical submergence predictions. Critical submergence equations used for comparison were ANSI and Yildirim (1998). The ANSI equation is shown in Equation 18.

$$\frac{S}{D} = 1.0 + 2.3 * Fr \tag{18}$$

where S is submergence, D is intake diameter, and Fr is Froude number in the intake. The predictive equation from Yildirim and Kocobas (1998) was previously described in Chapter II (Equation 16). The predictive equations were plotted on the same graph with the test result plot shown in Figure 14. The resulting chart is shown in Figure 16.

As seen in Figure 16, the critical submergence points from this study are near the theoretical Sc values and the experimental results where a vortex was present. The ANSI equation (Equation 16) bounds the tested values on the upper side. This indicates that it is a conservative value to use and agrees well with suggestions by researchers, including Yildirim and Kocobas (1995, 1998), to use a 10 percent factor of safety above the actual values for design to prevent air-core vortices. Yildirim's equation is much more intensive and is fitted with a polynomial trend line to aid in comparison to the tested

values. As seen in Figure 16, the tested values demonstrate a curve similar to that of Yildirim's equation.

Figure 15. Open configuration with air-core vortex.

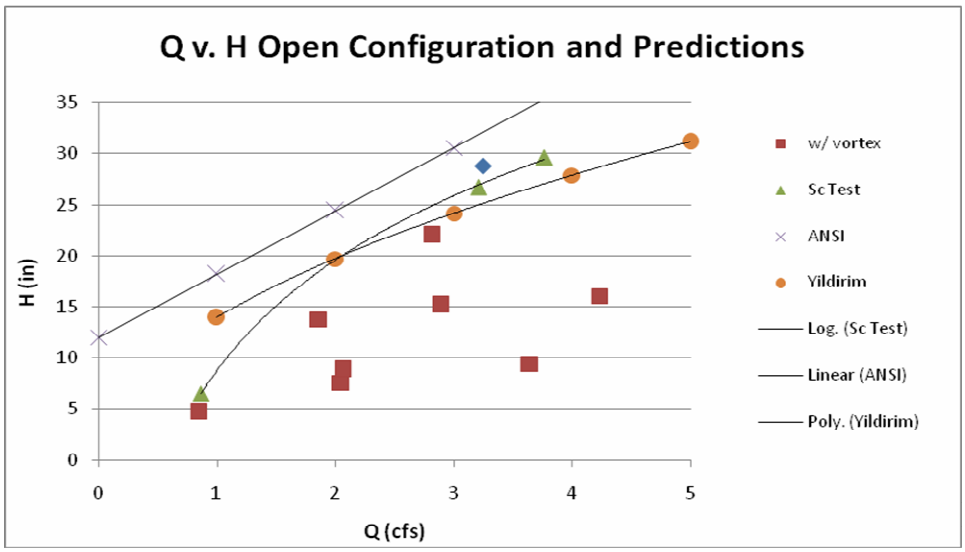

Figure 16. Open configuration and predictions from theory.

There are only three data points for the tested values curve, the shape of the curve is not necessarily reliable. As described previously, the test data indicate only the range within which the critical submergence is found, as such either the ANSI equation or the Yildirim equation lie within the same region for critical submergence obtained from this research.

Plate Configuration Results

The plate configuration was a small piece of the same light panel material used for the debris cages placed directly on the intake pipe across the opening. The plate configuration results are shown in Figure 17. No clear line was placed to approximate the critical submergence in these cases. The critical submergence for each plot would lie in the region between points of vortex occurrence and no vortex occurrence.

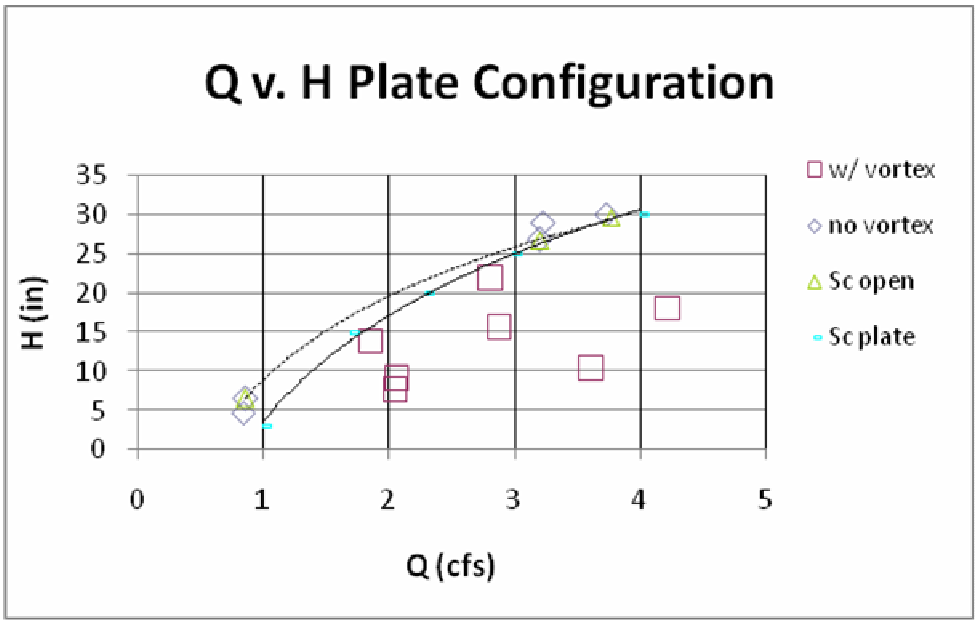

Fig 17. Plate configuration results.

An example of the plate configuration with an air core vortex is shown in Figure 18, as in visual observation the air core extending to the intake is difficult to see. It can be observed in the results plot for the plate configuration (Figure 17) that the placement of the grating plate directly on the intake pipe does not significantly change the critical submergence of the intake. In fact, the grating plate created worse vortices than the open configuration at submergences near the critical submergence. From observations in the testing, the plate was the only configuration which noticeably altered the head loss across the inlet. This was evidenced by a slight increase in the water surface elevation over all test conditions. The increase was small for the lower flow cases, on the order of 0.10 inches, and up to two inches in the model for the higher flow cases.

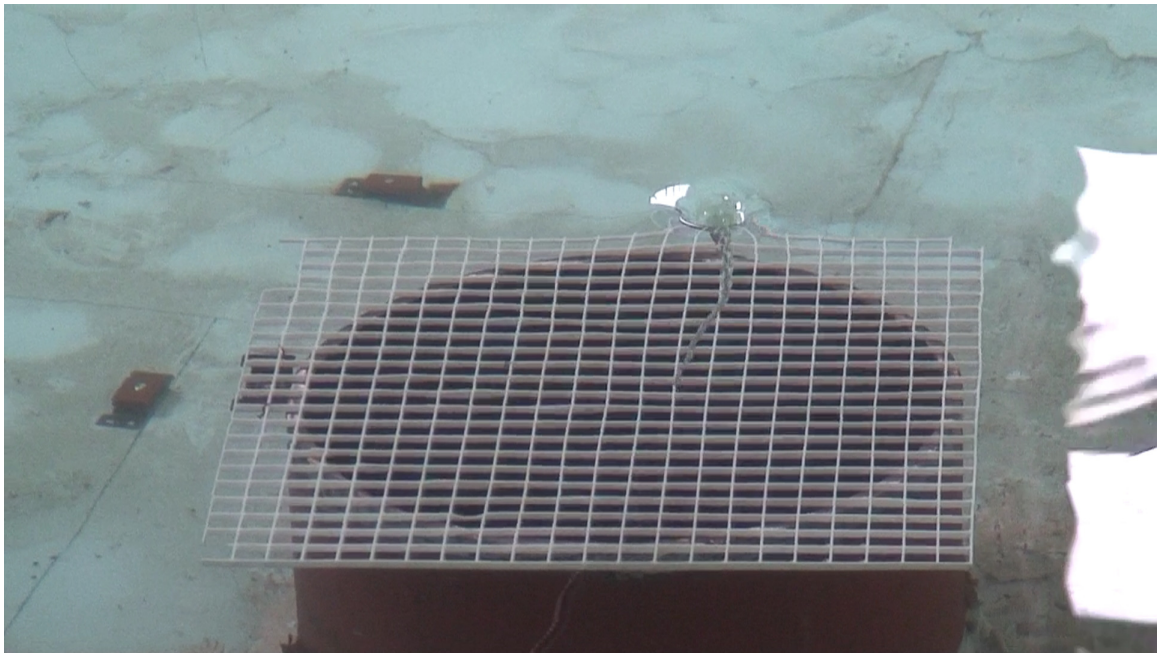

Figure 18. Plate configuration with air core vortex.

Debris Cage Results

The 24-in x 24-in x 18-in cage test results are shown in Figure 19, 24-in x 24-in x 24-in cage results are shown in Figure 20, 36-in x 36-in x 18-in cage results are shown in Figure 21, and 36-in x 36-in x 24-in cage results are shown in Figure 22.

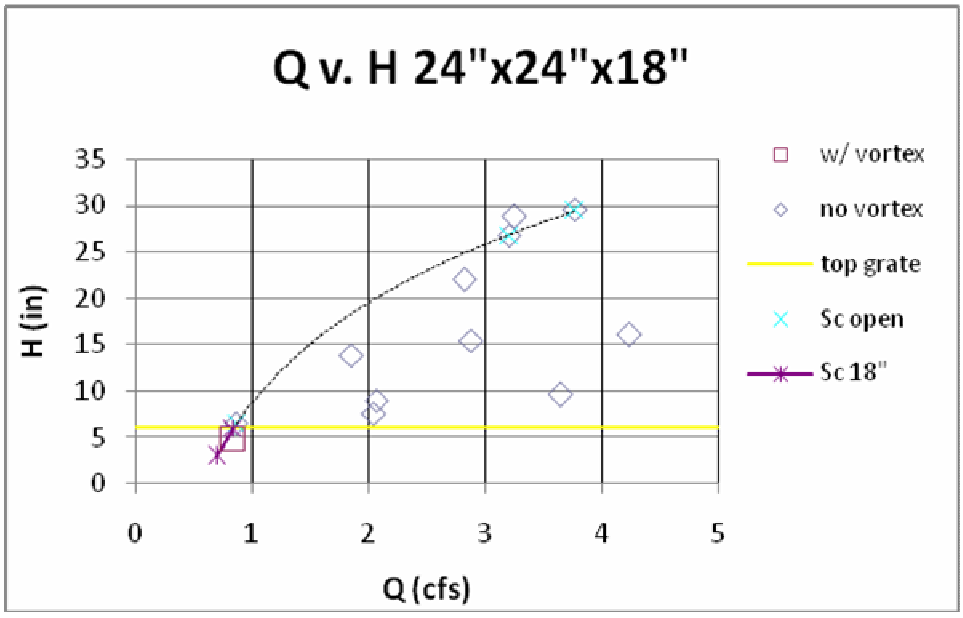

Figure 19. 24”x24”x18” debris cage results.

In the figures, the top of grate elevation is plotted for reference. It can be seen from the figures that the presence of the debris cages had a significant impact on the critical submergence of the intake. None of the flow conditions with water surface elevations above the top grate of the debris cage exhibited an air-core vortex. This indicates a significant critical submergence improvement for the air-core vortex over the open and plate configurations. Visual observation of the strength of circulation up to the dye-core vortex condition was indistinguishable from the open test configuration. Figure

23 is a photo of a tested configuration with a debris cage. The circulation and surface dimple are present, but no air-core vortex occurs. This photo is typical of the tested configurations with debris cages in place.

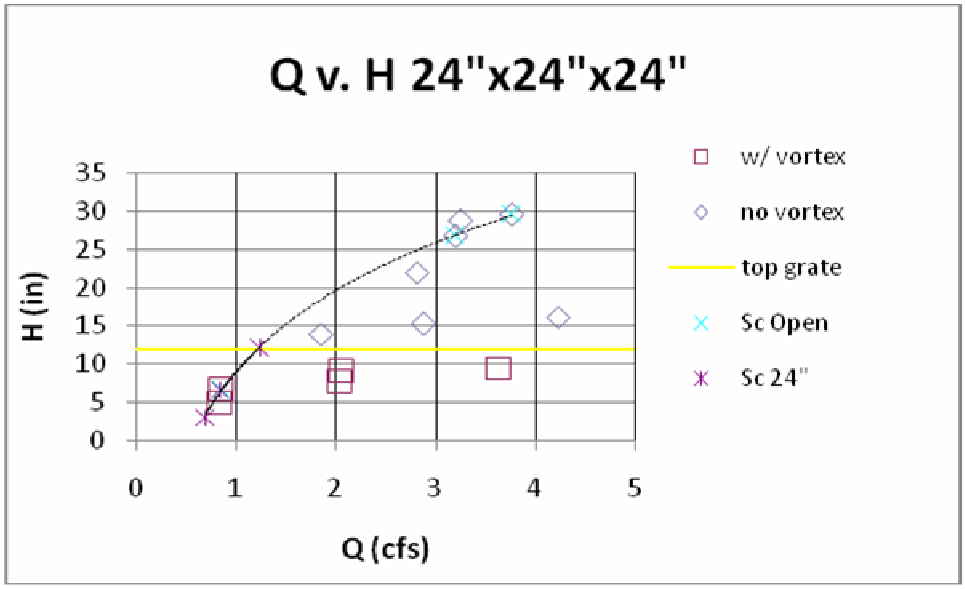

Figure 20. 24"x24"x24" debris cage results.

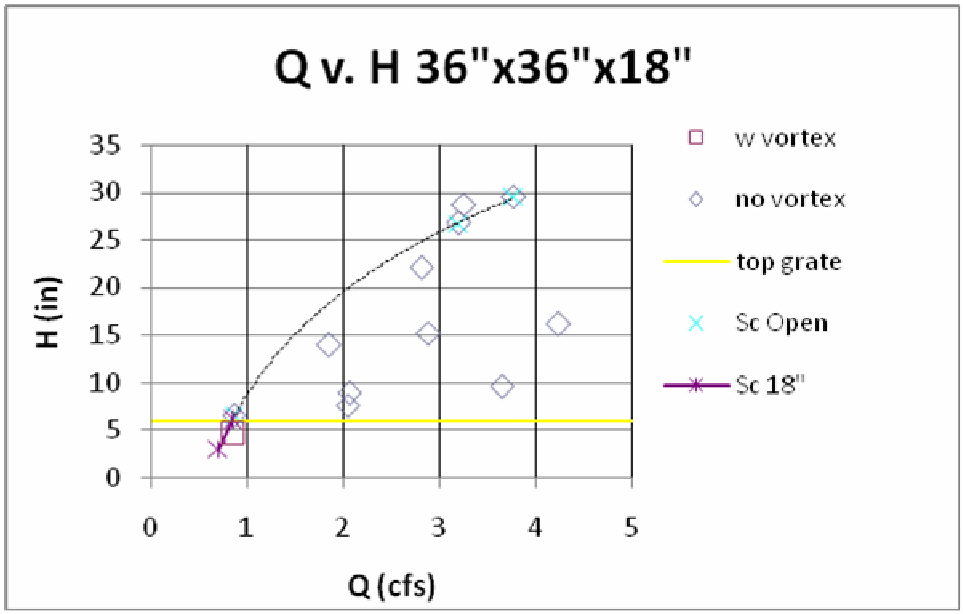

Figure 21. 36"x36"x18" debris cage results.

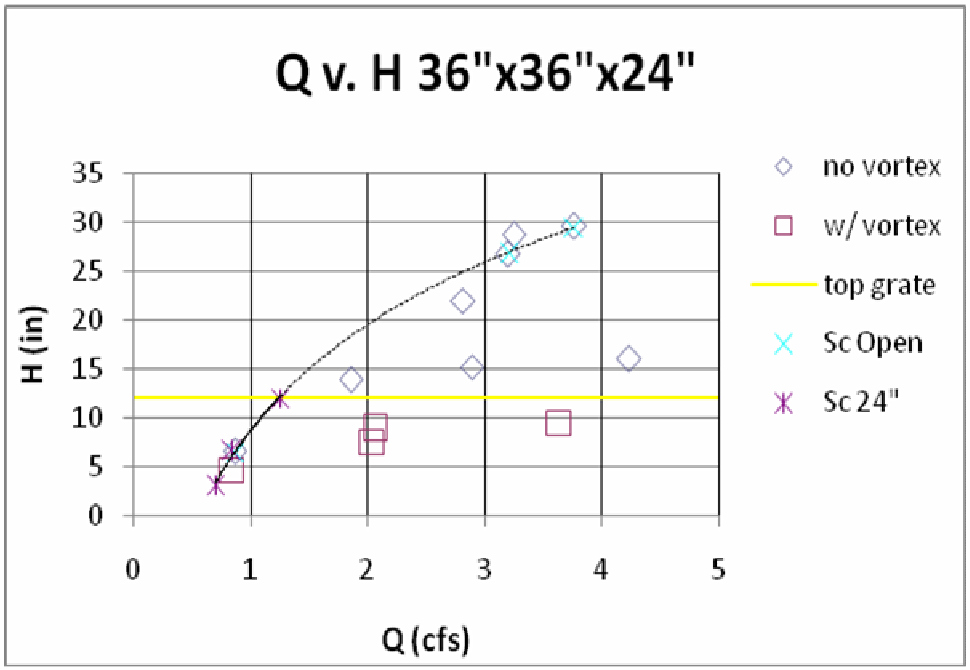

Figure 22. 36”x36”x24” debris cage results.

Figure 23. Debris cage with strong circulation and no air-core vortex.

Comparable flows for both the open configuration and the configurations with debris cages with the water surface elevation below the top grate of the cage resulted in the development of air-core vortices. There is a marked difference in vortex strength when the water surface is just above the top grate and when the water surface is just below the top grate. With the water surface just above the grate the flow exhibits, at most, a dye-core vortex. In the case with similar flow rate and the water surface just below the top grate a full air-core vortex to the inlet develops. This clear distinction demonstrates that the presence of the debris cage top grate is inhibiting air-core vortex development.

Comparison of Results

The only case in which a vortex occurred in the open configuration and not in the debris cage configuration with the water surface below the top grate occurred in test K (detailed in Appendix A). The open configuration appeared to be near S_c and considerable fluctuation was occurring in the vortex with multiple vortices observed interacting, dissipating, and reforming. The 24-in x 24-in x 18-in and 24-in x 24-in x 18-in debris cages, which have the same results since the water surface is below the top of both cages, exhibit a stronger stable vortex. This indicates that the presence of the side grates of the debris cages are influencing the flow in such a way that the vortex is able to become established and stable, where in the open case the surface waves and instability of the vortex are sufficient to prevent the vortex from reaching an established condition. The 36-in x 36-in x 18-in and 36-in x 36-in x 24-in debris cages exhibited no vortex and

no visible surface effects, including circulation. This would indicate that the debris cage side grates are influencing the approach flow. Determination of the specific influence of debris cage side grates on air-core vortex development cannot be derived from the results of this study.

The critical submergence approximation plots for each of the configurations are expressed in Figure 24. The 24-in x 24-in x 18-in and 36-in x 36-in x 18-in plots are approximately the same and are plotted together, as are the 24-in x 24-in x 24-in and 36-in x 36-in x 24-in plots. Each of the debris cage configurations are shown following the open configuration plot until the reservoir elevation exceeds the top grate elevation for the respective configurations, at which point they follow the top grate elevation. The

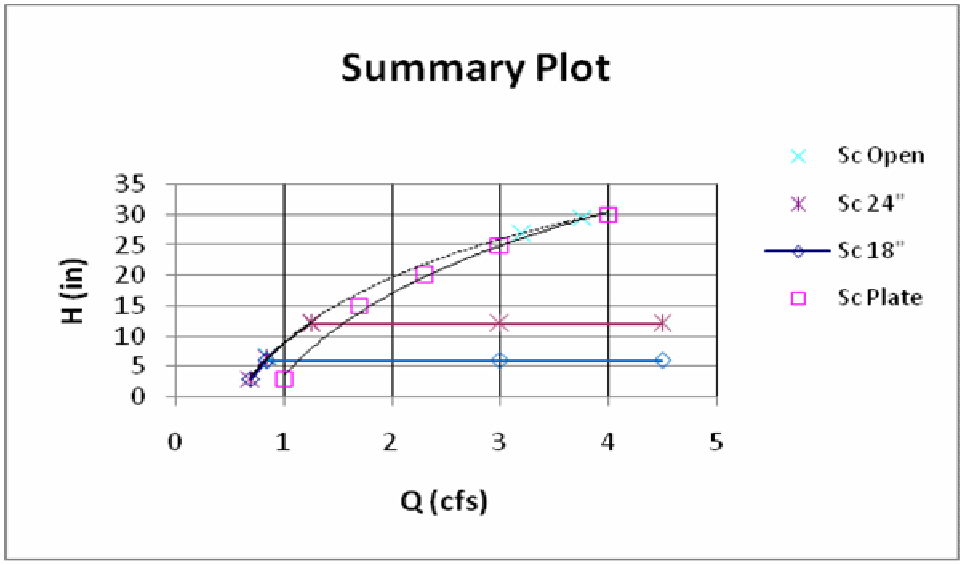

Figure 24. Critical submergence summary plot.

critical submergence for the plate configuration is slightly lower than that of the open configuration, more expressly so at lower flows.

From the results shown in Figure 22 it can be seen that the plate configuration has only a slight influence on the critical submergence of the air-core vortex. The improvement in critical submergence for air-core vortices was significant for each of the debris cage configurations, reducing the critical submergence to the elevation of the top grate of each cage.

Varying Top Grate Configuration

Six different top grate configurations were all tested in the 24-in x 24-in x 18-in debris cage at a flow rate of 2.95 cfs and reservoir head above the intake of approximately 11 inches. The original debris cage top grate, the open condition, and the debris cage without a top grate were also tested for comparison. The results are summarized in Appendix C. The open configuration had an air-core vortex to the intake, as did the debris cage with no top grate. The configurations with one slat across the center, two slats in a cross, three slats in parallel, and the top grate with the largest openings all had some degree of air-core vortex that fluctuated. The debris cage top grate with the smallest openings had some improvement over the original debris cage top grate and the second largest had improvement over both. The large opening top grate showed improvement over the three slats in parallel. This indicates that top grate members oriented in both directions are desirable for air-core vortex suppression.

The conclusion reached from this test is that the debris cage openings should be less than 15 percent of the diameter of the intake. In a debris cage configuration, this

dimension would likely be larger than the spacing desired to prevent debris entering the intake. In designing a debris cage for a vertical intake, the bars should be placed at the maximum spacing for the desired debris blockage up to 15 percent of the diameter. If feasible, bars oriented in both directions would further improve air-core vortex suppression.

Submerged Raft Comparison

In the additional test representing a submerged raft configuration, the original top grate of 24-in x 24-in light panel grating was suspended above the intake at the same elevation as the top grate on the debris cage. The resulting flow condition exhibited only a large circulation zone, with no vortex present and no surface dimple. This was the best performance of any configuration tested. The lack of side grates may result in reduction of flow restriction in that zone. Therefore, more of the flow passes into the intake below the level of the submerged grate. With less flow passing through the grate, there is a lessening of circulation and air-core vortex potential above the intake. Further investigation would be required to determine the optimal dimensions of the submerged raft. A submerged raft is not a debris cage, but a vortex suppression device. This study did not attempt to investigate vortex suppression devices specifically. The purpose herein is to determine to what extent debris cages can serve a secondary function by suppressing air-core vortices.

CHAPTER V

CONCLUSIONS

The critical submergence of the air-core vortex is significantly improved by the presence of a debris cage. Comparing the results from the open configuration to those of the configurations with debris cages shows that the presence of debris cages significantly reduces the critical submergence for the air-core vortex. In all of the configurations tested with the debris cages the air-core vortex was suppressed when the water surface was higher than the top grate of the debris cage. In observations of the flow conditions it was noted that the strength of circulation was not reduced by the debris cages to a degree that could be recognized visually, but the air-core vortex did not extend to the inlet or to the top of the cage.

As indicated by Anwar (1968), increasing the roughness within the zone of circulation reduces the strength of circulation, thus decreasing vortex strength. Observations indicate that the top grate of the debris cage influences the circulation above the intake by increasing the boundary roughness in the region of circulation. The interference of the debris cage top grating impedes the circulation near the top of the debris cage preventing the formation of the air-core vortex. If this is the controlling factor for the prevention of vortices in this study, the increase of viscous effects could introduce scale effects which would reduce the scalability of these results. Extreme care should be taken in model studies of debris cages, since scale effects introduced by the viscosity could result in different prototype performance from that observed in the scale model. By impeding the circulation just above the grate, the debris cage prevents an air-

core from developing to the inlet. More precise measurement of circulation differences would be helpful in verifying this conclusion, refining the precision of the results, and determining the degree of influence of the debris cage on dye-core vortices.

The presence of a vortex reduces the efficiency of flow passing through the inlet (Posey and Hsu, 1950). The reduction of flow efficiency in the zone of circulation above the intake could have the effect of causing more of the flow to pass into the intake from the sides of the debris cage. Reducing the portion of flow coming from directly above the intake has some similarity to placing a cap above the intake to force flow to the sides, one method employed for reducing critical submergence in a vertical intake (Gulliver, Rindels, and Lindblom, 1986).

At low water surface elevations and flow rates, the side grates had an influence on the development of vortices at the intake. However, the nature of this influence could not be determined from this research. At higher water surface elevations, above the top grate of the debris cage, the side grates could have some influence on the critical submergence of the intake. Measurements of velocity and circulation surrounding the intake with and without debris cages present may lead to improved understanding of the influence of debris cage side grates. In the testing of the submerged raft it was determined that the lack of side grates reduces the strength of circulation above the top grate. This could be a result of reduced flow blockage area. In this test, the submerged raft configuration performed better than any other tested configuration for suppression of air-core vortices and circulation reduction. Submerged rafts are one method recommended by some

researchers for the suppression of air-core vortices (ASCE, 1995). Submerged rafts are vortex suppression devices and are not the same as debris cages.

The conclusion that debris cages can prevent the air-core vortex at water surface elevations greater than the top grate does not reduce the necessity of model studies for vertical intakes. A multitude of factors influence the development of vortices at intakes. A real intake may have many characteristics differing from those tested in this study including; approach geometry, currents, wave action, stratified flow, and other variations. Model studies should be conducted for hydraulic intakes where vortices present a concern for safe operation. Model studies can aid in the proper design of debris cages to assist in vortex suppression at a vertical intake in still-water reservoir conditions.

The presence of a debris cage at a vertical intake in a still water reservoir greatly reduces the critical submergence of the air-core vortex. The debris cage has the potential to completely eliminate the air-core vortex for water surface elevations above the top grate of the debris cage. The strength of circulation observed at the surface of the flow did not appear to be reduced by the presence of the debris cage. Additional research would be required to quantify the influence of the debris cage on the circulation and determine if the debris cage has an influence on dye-core vortex strength. Inclusion of a debris cage in the design of a vertical intake has the potential benefit of reducing the critical submergence required to avoid air-core vortices.

REFERENCES

ASCE. 1995. Guidelines for design of intakes for hydroelectric plants. Committee on Hydropower Intakes of the Energy Division of ASCE, New York. 11 p.

Anwar, H.O. 1965. Flow in a free vortex. Water Power Apr. (1965):153-61.

Anwar, H.O. 1968. Prevention of vortices at intakes. Water Power Oct. (1968):393-401.

Daggett, L.L., and G.H. Keulegan. 1974. Similitude in free-surface vortex formations. Journal of the Hydraulics Division ASCE 100(HY11):1565-1581.

Daughtry, R.L. and Franzini, J.B. 1977. Fluid mechanics with engineering applications. McGraw-Hill N.Y. 7 p.

Gulliver, J.S., A.J. Rindels, and K.C. Lindblom. 1986. Designing intakes to avoid free-surface vortices. International Water Power and Dam Construction 38(9):24-28.

Hecker, G.E. 1981. Model-prototype comparison of free surface vortices. Journal of the Hydraulics Division ASCE 107(HY10):1243-1259.

Jain, A.K., K.G. Ranga Raju, and R.J. Garde. 1978. Vortex formation in vertical pipe intakes. Journal of the Hydraulics Division ASCE 104(10):1429-1445.

Knauss, J. 1987. Swirling flow problems at intakes. J. Knauss (editor, coordinator). IAHR, Balkema, Rotterdam.

Posey, C.J., and H.C. Hsu. 1950. How the vortex effects orifice discharge. Engineering-News Record 144(10):30.

Yildirim, N. and S.C. Jain. 1981. Surface tension effect on profile of a free vortex. Journal of the Hydraulics Division ASCE 107(1):132-136.

Yıldırım, N., and F. Kocabaş. 1995. Critical submergence for intakes in open channel flow. Journal of Hydraulic Engineering 121(12):900–905.

Yıldırım, N., and F. Kocabaş. 1998. Critical submergence for intakes in still-water reservoir. Journal of Hydraulic Engineering 124(1):103–104.

APPENDICES

Appendix A

Overflow Weir Calibration

The overflow weir was three inches wide and had adjustable blocks installed to allow any weir elevation within the height of the notch. The weir was calibrated using the four inch supply line. Four flows were passed over the overflow weir only and the data recorded in Table A1.

Cd was computed to be 0.585 by plotting the measured function and a theoretical function representing Equation A1. The results plot is shown below in Figure A1.

$$Q = \frac{2}{3} C_d \sqrt{2g} \cdot L \cdot H^{3/2} \qquad \text{(A1)}$$

Table A1. Overflow weir calibration data

Piezometer	Manometer	H over weir	DH	Q (cfs)
17.08	78.00	6.78	32.1041	0.3490
16.80	62.30	6.50	25.6421	0.3119
15.83	37.90	5.53	15.5993	0.2433
15.10	21.60	4.80	8.8904	0.1837

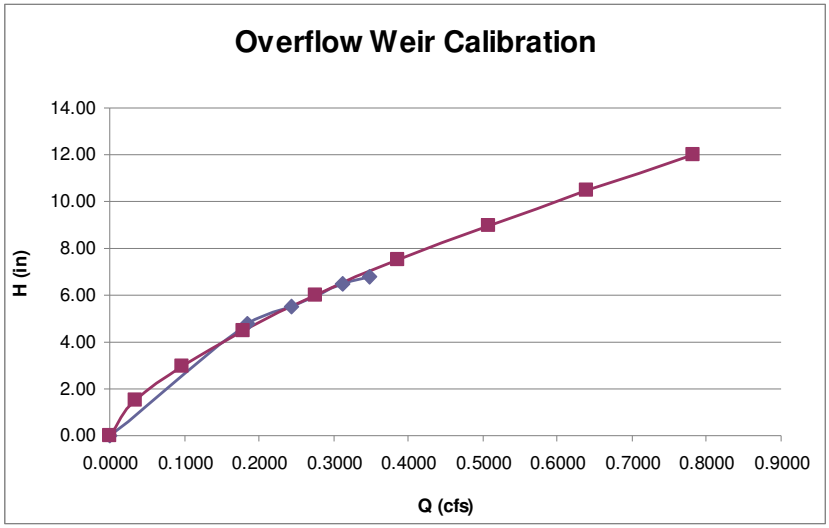

Figure A1. Overflow weir calibration plot.

Appendix B

Test Results Summary

Testing results are summarized in the following tables. Each table includes data collected and observations made regarding each of the test configurations and conditions.

Table B1. Test results A-C

Test #	Weir Elevation (in)	Inlet Valve	Manometer Fluid	Manometer Reading (cm)	Outlet Condition	Reservoir Elevation (in)	Air Core Vortex (Y/N)	Notes
A	19.65	8	Hg	37.85	Plate	21.85	Y	air core vortex to inlet
	19.65	8	Hg	38.00	24x18	22.00	N	small surface dimple, no vortex
	19.65	8	Hg	38.00	24x24	22.00	N	very small surface dimple
	19.65	8	Hg	38.00	36x18	22.03	N	small surface dimple
	19.65	8	Hg	38.00	36x24	22.02	N	tiny surface dimple
	19.65	8	Hg	38.00	Open	22.05	Y	air core vortex to inlet
B	14.3	8	Hg	38.55	Plate	15.50	Y	strong air core vortex, large spiral core, fluctuates to small air core
	14.3	8	Hg	38.6	24x18	15.45	N	rotation, 2.5 in. dimple, visible spiral approach flow
	14.3	8	Hg	38.6	24x24	15.25	N	no visible surface effects
	14.3	8	Hg	38.6	36x18	15.22	N	strong rotation, 3 in. dimple
	14.3	8	Hg	38.6	36x24	15.22	N	small surface dimple, migrating in circular pattern
	14.3	8	Hg	38.6	Open	15.20	Y	air core vortex, fluctuating, develops dissipates & reforms
C	20.2	8	Hg	56.9	Plate	26.87	N	no surface effects (vortex forms initially, then dissipates)
	20.2	8	Hg	56.65	24x18	26.78	N	med to small dimple w/ rotation
	20.2	8	Hg	56.65	24x24	26.75	N	very small dimple, slow rotation
	20.2	8	Hg	56.65	36x18	26.73	N	1.5" dimple
	20.2	8	Hg	56.65	36x24	26.75	N	0.75" dimple
	20.2	8	Hg	56.65	Open	26.72	Y	3" air core vortex, med-fine air core, dissipates and reforms

Table B2. Test results D-F

Test #	Weir Elevation (in)	Inlet Valve	Manometer Fluid	Manometer Reading (cm)	Outlet Condition	Reservoir Elevation (in)	Air Core Vortex (Y/N)	Notes
D	22.3	8	Hg	57.9	Plate	29.03	N	vortex initially forms but dissipates after stabilization
	22.3	8	Hg	57.9	24x18	28.73	N	2-3" surface dimple
	22.3	8	Hg	57.9	24x24	28.73	N	no surface effects
	22.3	8	Hg	57.9	36x18	28.73	N	2-3" surface dimple
	22.3	8	Hg	57.9	36x24	28.73	N	surface rotation visible, no dimple
	22.3	8	Hg	57.9	Open	28.76	N	1" surface dimple
E	9.15	8	Hg	60.8	Plate	10.35	Y	fluctuating from surface dimple to vortex to inlet
	9.15	8	Hg	60.8	24x18	9.60	N	2-3" dimple, no air core
	9.15	8	Hg	60.8	24x24	9.50	Y	1-2" vortex w/ fine air core to inlet (inside cage)
	9.15	8	Hg	60.8	36x18	9.55	N	2-3" dimple, no air core
	9.15	8	Hg	60.8	36x24	9.50	Y	1-2" vortex w/ fine air core to inlet (inside cage)
	9.15	8	Hg	60.8	Open	9.45	Y	strong air core vortex, med size
F	9.2	8	Hg	19.15	Plate	13.98	Y	2" vortex w/ fine air core to inlet
	9.2	8	Hg	19.15	24x18	13.88	N	1.5" dimple w/ rotation, no vortex
	9.2	8	Hg	19.15	24x24	13.90	N	no dimple, slow rotation visible
	9.2	8	Hg	19.15	36x18	13.90	N	1" dimple w/ rotation
	9.2	8	Hg	19.15	36x24	13.90	N	no dimple, slow rotation visible
	9.2	8	Hg	19.15	Open	13.80	Y	2" vortex w. med fine air core to inlet

Table B3. Test results G-I

Test #	Weir Elevation (in)	Inlet Valve	Manometer Fluid	Manometer Reading (cm)	Outlet Condition	Reservoir Elevation (in)	Air Core Vortex (Y/N)	Notes
G	9.2	8	Hg	19.45	Plate	9.00	Y	1.5" vortex w/ med. air core, some fluctuation
	9.2	8	Hg	19.45	24x18	9.00	N	1" surface dimple, occasional multiple dimples
	9.2	8	Hg	19.45	24x24	8.95	Y	1.5" vortex w/ med. Air core
	9.2	8	Hg	19.45	36x18	8.90	N	3" shallow depression, visible rotation
	9.2	8	Hg	19.45	36x24	8.90	Y	1.5" vortex w/ med air core to inlet
	9.2	8	Hg	19.45	Open	8.87	Y	1.5" vortex w/ med air core, similar to 24"h cages
H	6.4	8	Hg	19.6	Plate	7.62	Y	1.5" vortex w/ med-fine air core, fluctuating
	6.4	8	Hg	19.6	24x18	7.62	N	3" depression, visible rotation
	6.4	8	Hg	19.6	24x24	7.60	Y	steady vortex, med to large air core (large at upper and small at inlet)
	6.4	8	Hg	19.6	36x18	7.60	N	3.5" depression, visible rotation
	6.4	8	Hg	19.6	36x24	7.60	Y	1" vortex w/ fine air core to inlet
	6.4	8	Hg	19.6	Open	7.55	Y	1.5" vortex w/ med-fine air core
I	22.2	20	Blue	19	Plate	30.08	N	med-fine vortex occurs immediately but dissipates to 0.75" dimple
	22.2	20	Blue	19	24x18	29.55	N	1" surface dimple
	22.2	20	Blue	19	24x24	29.57	N	small depression w/ slow rotation, dimples at edge of cage
	22.2	20	Blue	19	36x18	29.57	N	2.5" surface dimple
	22.2	20	Blue	19	36x24	29.58	N	2" surface depression w/ slow rotation
	22.2	20	Blue	19	Open	29.57	Sc	2" vortex w/ fine air core to inlet, fluctuating w/in inches of surface (Sc)

Table B4. Test results J-L

Test #	Weir Elevation (in)	Inlet Valve	Manometer Fluid	Manometer Reading (cm)	Outlet Condition	Reservoir Elevation (in)	Air Core Vortex (Y/N)	Notes
J	22.2	20	Blue	19.8	Plate	18.10	Y	1" vortex, med-fine air core to inlet
	22.2	20	Blue	19.8	24x18	16.10	N	1.5" surface dimple, no air core
	22.2	20	Blue	19.8	24x24	16.17	N	small depression, strong rotation
	22.2	20	Blue	19.8	36x18	16.15	N	3" dimple, strong rotation, no air core
	22.2	20	Blue	19.8	36x24	16.10	N	small depression, med rotation
	22.2	20	Blue	19.8	Open	16.05	Y	steady 1.5" vortex, med air core to inlet
K	2.15	8	Hg	4.9	Plate	6.55	N	1" surface dimple, no air core
	2.15	8	Hg	4.9	24x18	6.55	N	no surface effects visible, w.s. just above top grate
	2.15	8	Hg	4.9	24x24	6.54	Y	2" vortex w/ steady air core
	2.15	8	Hg	4.9	36x18	6.55	N	no surface effects visible, w.s. just above top grate
	2.15	8	Hg	4.9	36x24	6.55	N	no surface effects visible
	2.15	8	Hg	4.9	Open	6.53	Sc	At Sc, vortex forms w/ intermittent air core, dissipates, & fluctuates
L	0	8	Hg	4.9	Plate	4.73	N	3" dimple w/ med-strong rotation, no air core
	0	8	Hg	4.9	24x18	4.70	Y	1.5" vortex, steady large top, fine lower air core
	0	8	Hg	4.9	24x24	4.70	Y	1.5" vortex, steady large top, fine lower air core
	0	8	Hg	4.9	36x18	4.70	Y	1" vortex w/ fine air core
	0	8	Hg	4.9	36x24	4.70	Y	1" vortex w/ fine air core
	0	8	Hg	4.9	Open	4.70	Y	0.75" dimple to fine vortex w/ bubble stream

Table B5. Test results varying top grates

Test #	Weir Elevation (in)	Inlet Valve	Manometer Fluid	Manometer Reading (cm)	Outlet Condition	Reservoir Elevation (in)	Air Core Vortex (Y/N)	Notes
R1	10.5	8	Hg	39.9	Open	990.98	Y	2" med. Vortex to intake
	10.5	8	Hg	39.9	Original Plate	991	N	3-4" surface dimple, medium circulation, no air core
	10.5	8	Hg	39.9	No plate	991.03	Y	3" strong steady air core vortex, med to large in size
	10.5	8	Hg	39.9	Fine plate	990.95	N	1-1/2" dimple, mild-med circulation, no air-core
	10.5	8	Hg	39.9	Med. Plate	990.03	N	small dimple, very mild circulation
	10.5	8	Hg	39.9	Course plate	990.93	Y	2" dimple, med circulation, air core vortex begins to form, then breaks up
	10.5	8	Hg	39.9	3 slats III	990.93	Y	med-large intermittent air-core vortex
	10.5	8	Hg	39.9	1 slat I	990.93	Y	med-large air-core vortex, transitions from one side to other
	10.5	8	Hg	39.9	2 slats +	990.93	Y	med-fine air-core vortex, transitions between quadrants
	10.5	8	Hg	39.9	subm. Raft	990.98	N	4" surface dimple, mild circulation

Appendix C

Calculations

Calculations were made from the collected test data to compute the outflow through the intake by first computing the inflow and overflow weir flow. Inflow was computed from calibration data previously collected at the UWRL for the orifice plates and U-tube manometers, shown in Table C1.

Using the values from Table C1 and the differential head (DH) computed from manometer readings for each test the inflow was computed as shown in Equation C1.

$$Q_{in} = C \cdot A_o \cdot \sqrt{\frac{2 \cdot g \cdot DH}{1 - \beta^4}} \qquad \text{(C1)}$$

The overflow weir flow rate was computed using the calibration data detailed in Appendix A, and applying Equation A1. Using continuity the flow through the test outlet pipe was computed as shown in Equation C2.

$$Q_{in} - Q_{overflow} = Q_{outlet} \qquad \text{(C2)}$$

Froude, Reynolds, and Weber numbers were also calculated and compared to the limiting criteria for model scale effects. Computations are shown in subsequent Tables C2-C4.

Table C1. Calibrated inflow measurement criteria

Size	D	d	Beta	Ao	C
4-inch	4.026	1.500	0.373	0.0123	0.6197
8-inch	7.981	5.000	0.626	0.1364	0.6106
20-inch	19.250	14.016	0.728	1.0715	0.6029
Weir Cd=	0.585		Specific gravity Blue =	1.7380	
			Specific gravity Hg =	13.6385	

Table C2. Computations for open and plate configurations

Test #	Outlet Condition	Beta	Ao	C	DH	Q Inflow (cfs)	Q Weir (cfs)	Q Outflow (cfs)	Froude	Reynolds	Weber
D	Open	0.6265	0.1364	0.6106	24.01	3.56	0.31	3.25	0.73	214216.06	6408.27
K	Open	0.6265	0.1364	0.6106	2.03	1.03	0.17	0.86	0.19	56871.53	451.68
C	Open	0.6265	0.1364	0.6106	23.49	3.52	0.31	3.21	0.72	211385.60	6240.04
I	Open	0.7281	1.0715	0.6029	0.46	4.14	0.38	3.77	0.85	248477.30	8622.04
L	Open	0.6265	0.1364	0.6106	2.03	1.03	0.19	0.84	0.19	55602.86	431.75
F	Open	0.6265	0.1364	0.6106	7.94	2.05	0.19	1.86	0.42	122671.10	2101.46
H	Open	0.6265	0.1364	0.6106	8.13	2.07	0.02	2.05	0.46	134955.92	2543.43
G	Open	0.6265	0.1364	0.6106	8.06	2.06	0.00	2.06	0.46	135962.50	2581.52
A	Open	0.6265	0.1364	0.6106	15.76	2.88	0.07	2.81	0.63	185430.37	4801.74
B	Open	0.6265	0.1364	0.6106	16.01	2.90	0.02	2.89	0.65	190477.97	5066.71
E	Open	0.6265	0.1364	0.6106	25.21	3.65	0.00	3.64	0.82	240183.25	8056.05
J	Open	0.7281	1.0715	0.6029	0.48	4.23	0.00	4.23	0.95	278991.64	10869.73
L	Plate	0.6265	0.1364	0.6106	2.03	1.03	0.19	0.84	0.19	55481.65	429.87
K	Plate	0.6265	0.1364	0.6106	2.03	1.03	0.17	0.86	0.19	56793.55	450.44
C	Plate	0.6265	0.1364	0.6106	23.59	3.53	0.32	3.20	0.72	211180.26	6227.92
D	Plate	0.6265	0.1364	0.6106	24.01	3.56	0.33	3.23	0.72	212925.86	6331.31
I	Plate	0.7281	1.0715	0.6029	0.46	4.14	0.42	3.73	0.84	245856.93	8441.15
B	Plate	0.6265	0.1364	0.6106	15.98	2.90	0.02	2.88	0.65	189782.35	5029.77
F	Plate	0.6265	0.1364	0.6106	7.94	2.05	0.20	1.85	0.42	121945.75	2076.68
H	Plate	0.6265	0.1364	0.6106	8.13	2.07	0.03	2.04	0.46	134814.14	2538.09
G	Plate	0.6265	0.1364	0.6106	8.06	2.06	0.00	2.06	0.46	135962.50	2581.52
A	Plate	0.6265	0.1364	0.6106	15.69	2.88	0.06	2.82	0.63	185619.27	4811.52
E	Plate	0.6265	0.1364	0.6106	25.21	3.65	0.02	3.62	0.81	238756.39	7960.61
J	Plate	0.7281	1.0715	0.6029	0.48	4.23	0.00	4.23	0.95	278991.64	10869.73

Table C3. Computations for 24-in x 24-in x 18-in and 24-in x 24-in x 24-in configurations

Test #	Outlet Condition	Beta	Ao	C	DH	Q Inflow (cfs)	Q Weir (cfs)	Q Outflow (cfs)	Froude	Reynolds	Weber
K	24x18	0.6265	0.1364	0.6106	2.03	1.03	0.17	0.86	0.19	56793.55	450.44
F	24x18	0.6265	0.1364	0.6106	7.94	2.05	0.19	1.86	0.42	122350.44	2090.49
H	24x18	0.6265	0.1364	0.6106	8.13	2.07	0.03	2.04	0.46	134814.14	2538.09
G	24x18	0.6265	0.1364	0.6106	8.06	2.06	0.00	2.06	0.46	135962.50	2581.52
B	24x18	0.6265	0.1364	0.6106	16.01	2.90	0.02	2.88	0.65	190007.29	5041.70
A	24x18	0.6265	0.1364	0.6106	15.76	2.88	0.07	2.81	0.63	185573.75	4809.16
C	24x18	0.6265	0.1364	0.6106	23.49	3.52	0.32	3.20	0.72	211099.87	6223.18
D	24x18	0.6265	0.1364	0.6106	24.01	3.56	0.31	3.25	0.73	214357.77	6416.75
E	24x18	0.6265	0.1364	0.6106	25.21	3.65	0.01	3.64	0.82	240012.61	8044.60
I	24x18	0.7281	1.0715	0.6029	0.46	4.14	0.37	3.77	0.85	248578.26	8629.05
J	24x18	0.7281	1.0715	0.6029	0.48	4.23	0.00	4.23	0.95	278991.64	10869.73
L	24x18	0.6265	0.1364	0.6106	2.03	1.03	0.19	0.84	0.19	55602.86	431.75
F	24x24	0.6265	0.1364	0.6106	7.94	2.05	0.19	1.85	0.42	122269.85	2087.73
B	24x24	0.6265	0.1364	0.6106	16.01	2.90	0.02	2.89	0.65	190388.49	5061.95
A	24x24	0.6265	0.1364	0.6106	15.76	2.88	0.07	2.81	0.63	185573.75	4809.16
C	24x24	0.6265	0.1364	0.6106	23.49	3.52	0.32	3.20	0.72	211242.90	6231.62
D	24x24	0.6265	0.1364	0.6106	24.01	3.56	0.31	3.25	0.73	214357.77	6416.75
I	24x24	0.7281	1.0715	0.6029	0.46	4.14	0.38	3.77	0.85	248477.30	8622.04
J	24x24	0.7281	1.0715	0.6029	0.48	4.23	0.00	4.23	0.95	278991.64	10869.73
L	24x24	0.6265	0.1364	0.6106	2.03	1.03	0.19	0.84	0.19	55602.86	431.75
K	24x24	0.6265	0.1364	0.6106	2.03	1.03	0.17	0.86	0.19	56832.56	451.06
H	24x24	0.6265	0.1364	0.6106	8.13	2.07	0.02	2.05	0.46	134855.08	2539.63
G	24x24	0.6265	0.1364	0.6106	8.06	2.06	0.00	2.06	0.46	135962.50	2581.52
E	24x24	0.6265	0.1364	0.6106	25.21	3.65	0.00	3.64	0.82	240130.22	8052.49

Table C4. Computations for 36-in x 36-in x 18-in and 36-in x 36-in x 24-in configurations

Test #	Outlet Condition	Beta	Ao	C	DH	Q Inflow (cfs)	Q Weir (cfs)	Q Outflow (cfs)	Froude	Reynolds	Weber
K	36x18	0.6265	0.1364	0.6106	2.03	1.03	0.17	0.86	0.19	56793.55	450.44
F	36x18	0.6265	0.1364	0.6106	7.94	2.05	0.19	1.85	0.42	122269.85	2087.73
H	36x18	0.6265	0.1364	0.6106	8.13	2.07	0.02	2.05	0.46	134855.08	2539.63
G	36x18	0.6265	0.1364	0.6106	8.06	2.06	0.00	2.06	0.46	135962.50	2581.52
B	36x18	0.6265	0.1364	0.6106	16.01	2.90	0.02	2.89	0.65	190442.47	5064.82
A	36x18	0.6265	0.1364	0.6106	15.76	2.88	0.07	2.81	0.63	185487.91	4804.72
C	36x18	0.6265	0.1364	0.6106	23.49	3.52	0.31	3.21	0.72	211338.07	6237.23
D	36x18	0.6265	0.1364	0.6106	24.01	3.56	0.31	3.25	0.73	214357.77	6416.75
E	36x18	0.6265	0.1364	0.6106	25.21	3.65	0.00	3.64	0.82	240073.26	8048.67
I	36x18	0.7281	1.0715	0.6029	0.46	4.14	0.38	3.77	0.85	248477.30	8622.04
J	36x18	0.7281	1.0715	0.6029	0.48	4.23	0.00	4.23	0.95	278991.64	10869.73
L	36x18	0.6265	0.1364	0.6106	2.03	1.03	0.19	0.84	0.19	55602.86	431.75
K	36x24	0.6265	0.1364	0.6106	2.03	1.03	0.17	0.86	0.19	56793.55	450.44
F	36x24	0.6265	0.1364	0.6106	7.94	2.05	0.19	1.85	0.42	122269.85	2087.73
B	36x24	0.6265	0.1364	0.6106	16.01	2.90	0.02	2.89	0.65	190442.47	5064.82
A	36x24	0.6265	0.1364	0.6106	15.76	2.88	0.07	2.81	0.63	185516.58	4806.20
C	36x24	0.6265	0.1364	0.6106	23.49	3.52	0.32	3.20	0.72	211242.90	6231.62
D	36x24	0.6265	0.1364	0.6106	24.01	3.56	0.31	3.25	0.73	214357.77	6416.75
I	36x24	0.7281	1.0715	0.6029	0.46	4.14	0.38	3.77	0.85	248426.77	8618.53
J	36x24	0.7281	1.0715	0.6029	0.48	4.23	0.00	4.23	0.95	278991.64	10869.73
L	36x24	0.6265	0.1364	0.6106	2.03	1.03	0.19	0.84	0.19	55602.86	431.75
H	36x24	0.6265	0.1364	0.6106	8.13	2.07	0.02	2.05	0.46	134855.08	2539.63
G	36x24	0.6265	0.1364	0.6106	8.06	2.06	0.00	2.06	0.46	135962.50	2581.52
E	36x24	0.6265	0.1364	0.6106	25.21	3.65	0.00	3.64	0.82	240130.22	8052.49

Table C5. Top grating variation test results

Test #	Outlet Condition	Beta	Ao	C	DH	Q Inflow (cfs)	Q Weir (cfs)	Q Outflow (cfs)	Froude	Reynolds	Weber
R1	Open	0.6265	0.1364	0.61	16.54	2.95	0.07	2.88	0.65	189890.96	5035.53
R2	Original Plate	0.6265	0.1364	0.61	16.54	2.95	0.07	2.88	0.65	189832.24	5032.42
R3	No plate	0.6265	0.1364	0.61	16.54	2.95	0.08	2.88	0.65	189743.71	5027.72
R4	Fine plate	0.6265	0.1364	0.61	16.54	2.95	0.07	2.88	0.65	189978.61	5040.18
R5	Med. Plate	0.6265	0.1364	0.61	16.54	2.95	0.08	2.88	0.65	189773.28	5029.29
R6	Course plate	0.6265	0.1364	0.61	16.54	2.95	0.07	2.88	0.65	190036.74	5043.26
R7	3 slats III	0.6265	0.1364	0.61	16.54	2.95	0.07	2.88	0.65	190036.74	5043.26
R8	1 slat I	0.6265	0.1364	0.61	16.54	2.95	0.07	2.88	0.65	190036.74	5043.26
R9	2 slats +	0.6265	0.1364	0.61	16.54	2.95	0.07	2.88	0.65	190036.74	5043.26
R10	subm. Raft	0.6265	0.1364	0.61	16.54	2.95	0.07	2.88	0.65	189890.96	5035.53

Appendix D

Reference Request

Mr. Davis:

I would like to request permission to reference SNWA project IPS3.2 regarding testing for intake #2 in my MS thesis at Utah State University. The reference is limited to the introduction regarding the observed suppression of vorticity at the intake by the model debris cage. Two photos from the testing are also included in the introduction. Thank you.

Sincerely,

Skyler Allen

From: Maria Gates [mailto:maria.gates@usu.edu]
Sent: Friday, April 11, 2008 9:17 AM
To: Davis, Ted/LAS
Subject: IPS3.2

Mr. Davis,

I am sending this email to request your permission for our graduate student, Skyler Allen (who has been working with Steve Barfuss on this project) to refer to the above project in his Master Thesis (please see attached request). The paper is in draft form and has not yet been read by his committee, as of yet. I will be happy to send you a copy of the report once it is published if you would like. Please let me know if you have any questions. I look forward to your response.

PS – Please forward this to any appropriate people

Sincerely,

Maria Gates
UWRL Business Office
(435) 797-3120
(435)797-3102 Fax(See attached file: Permission Request Letter.SA.pdf)

<Ted.Davis@CH2M.com>
04/14/2008 07:59 AM
To <Erika.Moonin@snwa.com>
cc
Subject FW: IPS3.2
Hi Erika,

We received a request from the graduate student who was helping on the Utah State University Model Testing. He wanted to reference the model for the Intake No. 2 debris deflector in his Master's thesis. I fully support graduate students when I can, but being SNWA's facility I wanted to be sure SNWA approved.

Thanks,
Ted

From: Robin.Rockey@snwa.com [mailto:Robin.Rockey@snwa.com]
Sent: Monday, April 14, 2008 10:19 AM
To: maria.gates@usu.edu
Cc: ted.davis@ch2m.com; Erika.Moonin@snwa.com
Subject: Reference Request

Ms. Gates:

Please forward to Mr. Skyler Allen our support and permission to reference the Southern Nevada Water Authority's Intake No. 2 project in his Master's Thesis. We would welcome the opportunity to review this reference prior to publication if desired.

Thank you,

Robin Rockey
Project Information
Southern Nevada Water Authority
(702) 862-3405 (phone)

Erika Moonin/LVVWD

----- Forwarded by Erika Moonin/LVVWD on 04/14/2008 08:29 AM -----